Article

Progressive unanchoring of Antarctic ice shelves since 1973

https://doi.org/10.1038/s41586-024-07049-0

Received: 24 March 2023

Accepted: 9 January 2024

Published online: 21 February 2024

Open access

Check for updates

Bertie W. J. Miles[1]✉ & Robert G. Bingham[1]

Mass loss of the Antarctic Ice Sheet has been driven primarily by the thinning of the floating ice shelves that fringe the ice sheet[1], reducing their buttressing potential and causing land ice to accelerate into the ocean[2]. Observations of ice-shelf thickness change by satellite altimetry stretch back only to 1992 (refs. 1,3–5) and previous information about thinning remains unquantified. However, extending the record of ice-shelf thickness change is possible by proxy, by measuring the change in area of the surface expression of pinning points—local bathymetric highs on which ice shelves are anchored[6]. Here we measure pinning-point change over three epochs spanning the periods 1973–1989, 1989–2000 and 2000–2022, and thus by proxy infer changes to ice-shelf thickness back to 1973–1989. We show that only small localized pockets of ice shelves were thinning between 1973 and 1989, located primarily in the Amundsen Sea Embayment and the Wilkes Land coastline. Ice-shelf thinning spreads rapidly into the 1990s and 2000s and is best characterized by the proportion of pinning points reducing in extent. Only 15% of pinning points reduced from 1973 to 1989, before increasing to 25% from 1989 to 2000 and 37% from 2000 to 2022. A continuation of this trend would further reduce the buttressing potential of ice shelves, enhancing ice discharge and accelerating the contribution of Antarctica to sea-level rise.

The contribution of the Antarctic Ice Sheet to global sea-level rise has been accelerating[7,8], enhancing the risk of flooding and other associated hazards to low-lying coastal communities[9]. Much of this mass loss has been attributed to warm ocean currents weakening the buttressing effects of its ice shelves[10–12], primarily in West Antarctica and the Wilkes Land coastline of East Antarctica[10–12], and hence driving an acceleration of ice discharge into the ocean[1,2]. Therefore, observational records that track the change in ice-shelf thickness over the longest possible time periods are important for explaining how the Antarctic Ice Sheet is changing and hence forecasting future mass loss. Existing records of ice-shelf thickness change derived from satellite altimetry span 30 years and have shown major ice-shelf thinning in some parts of West Antarctica and the western Antarctic Peninsula, thinning in the Wilkes Land sector of East Antarctica and limited change in most other ice shelves[3–5,12–14]. However, this satellite-altimetry record remains short relative to the typically multidecadal response times of many Antarctic ice shelves[15], and we do not know how widespread ice-shelf thinning was before 1992. Extending records of ice-shelf thickness change is important because a longer time series may directly help to lower uncertainties associated with the future contribution of Antarctica to global sea level by helping to calibrate numerical models[16,17].

Here, to extend the ice-shelf thickness change record to encompass the past 50 years, we implement a method that uses optical satellite imagery to track changes in the surface expression of pinning points that we treat as a proxy for ice-shelf thickness change (Fig. 1). Pinning points are common features around the Antarctic coastline that form when part of a floating ice shelf anchors onto a bathymetric high[6]: this interaction forms a bump on the otherwise smooth ice-shelf surface that is visible in optical imagery. Crucially, for the analysis presented here, the surface expression of this bump changes through time as an ice-shelf thickens or thins[10,18] in response to its altering proportion of contact with the underlying bedrock high (Fig. 1). Although we focus here mainly on the monitoring of pinning-point change as a proxy for changes in ice-shelf thickness, we also note that pinning points are fundamentally important to ice-sheet mass balance because they buttress portions of upstream ice flow and limit ice discharge into the ocean[19–21]. The pinning points can also play an important part in calving by promoting rifting[22,23], and they influence the spatial pattern of basal melt by altering ocean circulation beneath ice shelves[24]. For all of these reasons, understanding better the evolution of pinning points through the longest possible time periods is important. Here we have systematically tracked changes in the surface expression of pinning points around Antarctica since 1973 to provide the first pan-ice-sheet observation-based characterization of Antarctic ice-shelf thickness change for the past five decades.

Fifty years of pinning-point change

We used the full Landsat satellite-image archive to create two new near-cloud-free mosaics of the ice shelves of Antarctica for 1973 and 1989, with spatial resolutions of 60 m and 30 m, respectively (Methods and Extended Data Fig. 1). These two new mosaics represent our earliest near-cloud-free snapshots of the ice shelves of Antarctica. We used these mosaics, along with the existing Landsat-7 LIMA mosaic[25] from 2000, and Landsat-8 and Landsat-9 imagery from 2022, to track changes in the surface expression of pinning points from 1973–1989,

[1]School of GeoSciences, Edinburgh University, Edinburgh, UK. ✉e-mail: bertie.miles@ed.ac.uk

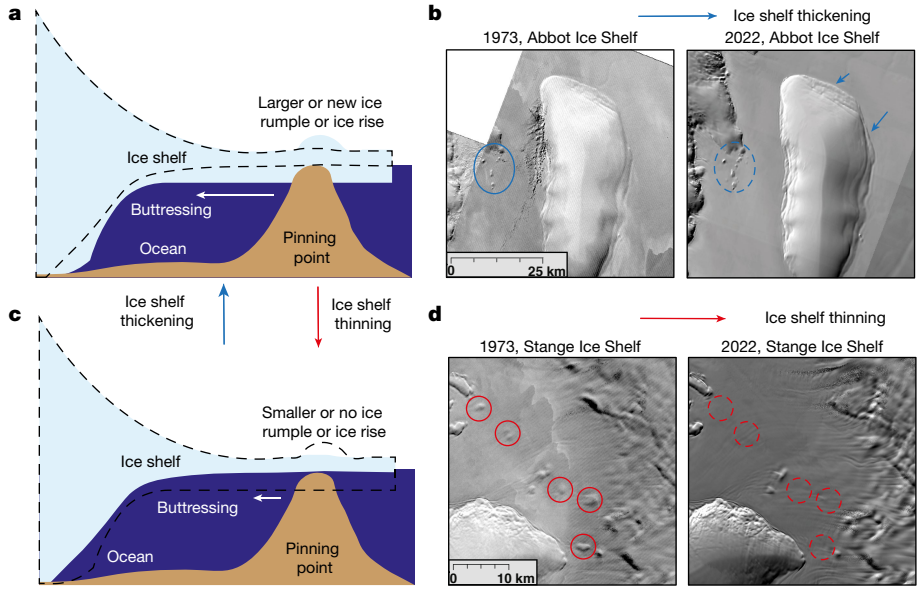

Fig. 1 | Schematic of processes that cause changes in the surface expression of pinning points. a, Ice-shelf thickening increases contact with the underlying bedrock high, causing the surface impression of the pinning point to increase in area. **b**, Example from Abbot Ice Shelf of ice-shelf thickening increasing the surface expression of pinning points between 1973 (Landsat-1 image) and 2022 (Landsat-8 image). **c**, Ice-shelf thinning reduces contact with the underlying bedrock high, causing the surface expression of the pinning point to decrease in area. The dotted lines represent the change in ice-shelf thickness. **d**, Example from Stange Ice Shelf of ice-shelf thinning reducing surface expression of pinning points between 1973 (Landsat-1 image) and 2022 (Landsat-8 image). Landsat imagery courtesy of the US Geological Survey. See Supplementary Animations for more examples. Scale bars, 25 km (**b**) and 10 km (**d**).

1989–2000 and 2000–2022, and to produce a long-term record of change between 1973 and 2022. We characterize the change in the surface expression of pinning points into three categories: smaller in extent, no detectable change and larger in extent.

A comparison between pinning-point change from 2000 to 2022 and ice-shelf thickness change derived from the ICESat and ICESat-2 satellites from 2003 to 2019 (ref. 13) shows a broad agreement in the spatial pattern of change (Methods and Extended Data Fig. 2). That is, the vast majority (86%) of pinning points that grew in area correspond to regions in which satellite altimetry recorded ice-shelf thickening (>0 m yr^{-1}), whereas 85% of pinning points that experienced no detectable change in area are in regions in which altimetry diagnosed limited change (between −1 m yr^{-1} and 1 m yr^{-1}) in ice-shelf thickness. A smaller proportion (66%) of the pinning points that reduced in extent correspond to regions of altimetry-detected ice-shelf thinning (<0 m yr^{-1}; Extended Data Fig. 3). Several factors might have driven this reduced correlation, including the ungrounding of pinning points causing short-term localized thickening downstream in the wake of the former pinning points and our cautious approach to classifying pinning-point change, that is, classifying pinning points as no detectable change in which there is ambiguity (Methods). However, in some rare instances, we suggest that the visible retreat of the grounding line from Landsat imagery and extensive nearby pinning-point loss are incompatible with simultaneous ice-shelf thickening, for example, George VI Ice Shelf (Extended Data Fig. 4a). This suggests that in rare, highly localized examples, satellite altimetry may not be capturing the true direction in ice-shelf thickness change. Comparing two different altimetry products[3,13] in highly localized areas, we also observe conflicting signals in the direction of ice-shelf thickness change (Extended Data Fig. 4). Overall, however, the broad agreement between pinning-point change and satellite altimetry within the overlapping time frames, coupled with theoretical considerations (Fig. 1), substantiates the role of our pinning-point observations from 1973 to 1989 and 1989 to 2000 as a proxy for ascertaining the direction of ice-shelf thickness change.

Having demonstrated the validity of using changes to the area of pinning points surrounding Antarctica as a proxy for changes to ice-shelf thickness, we present, in Fig. 2, the first observationally constrained estimates of pinning-point change across Antarctica through the 1970s and 1980s, which, in turn, enable us to infer ice-shelf thickness changes around the ice sheet over the past 50 years. These observations demonstrate that ice-shelf thinning was generally less extensive around much of Antarctica than has been observed since the early 1990s onwards from satellite altimetry. However, the observations show that even between 1973 and 1989 concentrated hotspots of ice-shelf thinning were underway in Amundsen Sea Embayment in West Antarctica and in Holmes, Moscow University and Totten ice shelves in East Antarctica, demonstrating that these ice shelves began to thin at least 50 years ago. Pinning-point loss and ice-shelf thinning subsequently spread, and this is characterized by 15% of all mapped pinning points reducing in extent from 1973 to 1989, increasing to 25% in 1989–2000 and 37% between 2000 and 2022. In the following sections, we focus on the regional variations in pinning-point change across the Antarctic Peninsula, West Antarctica and East Antarctica.

In the Antarctic Peninsula, all pinning points were lost following the collapse of Prince Gustav, Larsen A, Larsen B and Wordie ice shelves over the past 50 years (ref. 26) (Fig. 3). Further south and facing the Weddell Sea, there has been very little change to pinning on Larsen C and Larsen D ice shelves (Fig. 3). The only exception has been Bawden Ice Rise, located at the front of Larsen C ice shelf. An ice rise is a type of pinning point that diverts ice flow around it and is characterized by maintaining its own local flow regime[6]. At this ice rise, basal melt rates have been increasing[14] and our observations flag visible shrinkage since 1989. The ongoing ungrounding from this ice rise will have an impact on local ice flow[27], but the absence of any major changes elsewhere on the Larsen C ice shelf would suggest that there is a limited prospect of catastrophic disintegration anytime soon.

Ice shelves facing the Bellingshausen Sea, incorporating those in both the western Antarctic Peninsula and in West Antarctica, exhibited contrasting changes in pinning points, which can be attributed to the varying drafts of these ice shelves. The relatively thin Wilkins[28] and Abbot ice shelves[29] thickened from 1973 to 1989 and 1989 to 2000 (Fig. 3d and

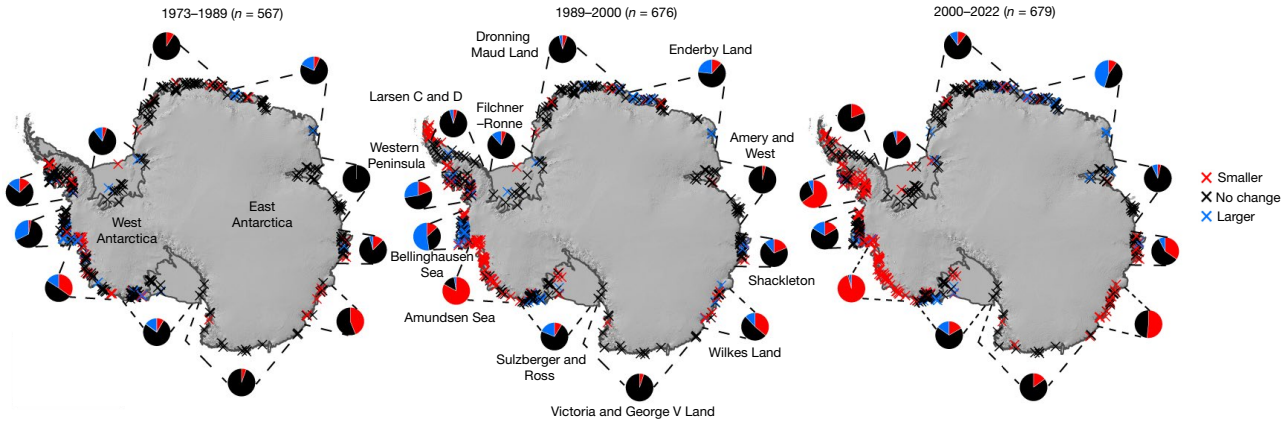

Fig. 2 | Pinning-point change over three epochs spanning the periods 1973–1989, 1989–2000 and 2000–2022. The pie charts represent the proportion of pinning points that reduced in area, remained the same or grew in area for each of the regions delineated by the dotted lines. The number of pinning points (*n*) mapped in each epoch is shown above each panel. Pie charts exclude data from collapsed ice shelves (Prince Gustav, Larsen A, Larsen B and Wordie). Mapped pinning-point change is overlain on the REMA mosaic of Antarctica[41].

Extended Data Fig. 5), whereas small sections of the relatively thick George VI[30], Stange and Venable[31] ice shelves were already thinning during this time period (Fig. 2). This implies that the thermocline on the continental shelf was deeper than the draft of Wilkins and Abbot ice shelves, but shallower than the drafts of George VI, Stange and Venable ice shelves allowing the warmer ocean water to facilitate basal melting. However, a clear shift in pattern occurred between 2000 and 2022, in which Wilkins and Abbott ice shelves transitioned to a more neutral pattern, with some pinning points continuing to grow, whereas others started to reduce in extent for the first time in the observational record. This is consistent with ocean observations from the 2000s, which place the thermocline at approximately the same depth as the mean draft of both Wilkins[28] and Abbot[29] ice shelves, which means the layer of warm water at the bottom of the ocean column would be able to intermittently reach the bases of these thinner ice shelves. At George VI, Stange and Venable ice shelves, much more widespread thinning took hold, with nearly every pinning point reducing in extent (Fig. 2). Collectively these patterns imply a decadal-scale raising of the thermocline depth and thickening of the layer of warm water on the continental shelf across the entire Bellingshausen Sea sector since 2000 that is consistent with ocean reanalysis products[32].

In the Amundsen Sea Sector in West Antarctica, 35% of pinning points reduced in area and 15% increased in area between 1973 and 1989 (Fig. 2). During this period, our results show that Pine Island Glacier, Thwaites, Dotson and Crosson ice shelves were already unanchoring from their pinning points and thinning decades before the earliest satellite-altimetry observations (Extended Data Figs. 6 and 7). This confirms that the processes driving the mass loss of West Antarctica have been underway for at least 50 years. Strong decadal variability in ocean forcing exists in this region and ocean-temperature data from the central tropical Pacific indicate that ocean conditions in the Amundsen Sea Sector were relatively cool during the mid-1970s to mid-1990s (ref. 11) (Extended Data Fig. 7), so we consider it that the pervasive thinning observed here was probably already well underway from before our records begin. This would be consistent with geological evidence that Pine Island Glacier began to retreat in the 1940s after its ice-shelf unanchored from a key pinning point[33], or possibly even earlier to coincide with the grounding-line retreat of Thwaites Glacier[34]. By contrast, further west on the Amundsen Sea coastline pinning points changed little between 1973 and 1989, with some even growing slightly in extent, and hence we did not detect evidence for ice-shelf thinning over much of the Getz Ice Shelf until the 1990s (Fig. 2 and Extended Data Fig. 7). Pinning-point loss markedly spread between 1989 and 2000, with 83% of pinning points reducing in area, and only the far western section of Getz Ice Shelf escaping major pinning-point loss and ice-shelf thinning. In 2000–2022, 94% of all remaining pinning points in the Amundsen Sea Sector reduced in area (Fig. 2 and Extended Data Fig. 7), consistent with the widespread ice-shelf thinning diagnosed by satellite altimetry[3,13].

In Marie Byrd Land, amidst a general trend for little pinning-point change, our observations highlight notable pinning-point loss on Hull Glacier between 1973 and 1989. The presence of a heavily damaged ice tongue on Hull Glacier in 1973 may suggest a more prominent ice tongue in the years or decades before (Extended Data Fig. 6) and would imply that Hull Glacier was one of the few glaciers in Antarctica to be thinning in the 1970s. This long-term thinning may help to explain its recent rapid acceleration and grounding-line retreat[35]. At the heavily pinned Sulzberger Ice Shelf, very little change has occurred over the past five decades, although pinning-point loss near the grounding line (Fig. 2) suggests that warm water is now capable of reaching the grounding line and may represent the precursor to more widespread thinning across the ice shelf. Further west again, several pinning points grew substantially on the Swinburne Ice Shelf, in which we estimate that parts of the ice shelf have thickened upwards of 30 m (Extended Data Fig. 5). Across the Ross Ice Shelf, most pinning points changed very little, but Steershead Ice Rise and two other large ice rises located downstream of Kamb Ice Stream shrank consistently (Fig. 3e). Thus, our observations validate numerical models that have predicted a thinning of this section of the Ross Ice Shelf in response to the shutdown of Kamb Ice Stream[36]. We also observe between 2000 and 2022 a 5-km retreat of Engelhardt Ice Ridge, at the junction between Kamb and Whillans ice streams, continuing a longer-term retreat from at least the 1960s (ref. 37).

In East Antarctica, major pinning-point loss over the past 50 years has been concentrated around the fringes of Wilkes Land (Figs. 2 and 3). However, unlike for West Antarctica and the Antarctic Peninsula, there has been no clear acceleration in the proportion of pinning points reducing in area. There has been a reduction in pinning throughout each of our three epochs at Holmes Ice Shelf (Fig. 3c), highlighting the long-term thinning of this ice shelf. At Moscow University Ice Shelf, 6 km of erosion has occurred from an elongated ice rise that separates the ice shelf and the open ocean between 1973 and 2000. The shrinkage of this ice rise has been so extensive that it has allowed a new ice-shelf tributary to develop across its southern flank (Fig. 3b). Continued melting of this ridge could cause a major change in the flow direction of the entire ice shelf resulting in a substantial change in

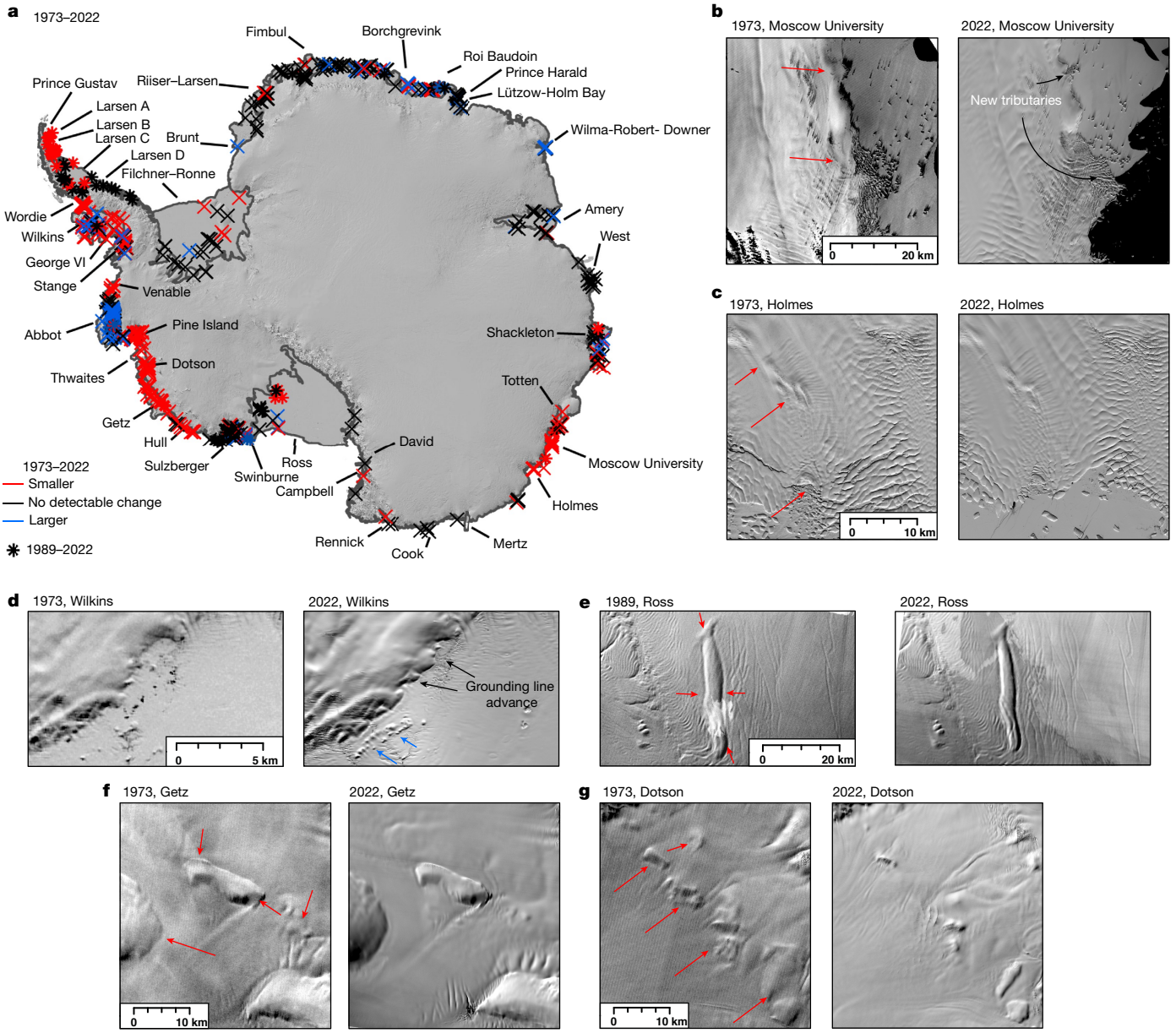

Fig. 3 | Antarctic pinning-point change from 1973 to 2022. a, Mapped pinning-point change from 1973 to 2022 overlain on the REMA mosaic of Antarctica[41]. Asterisks represent regions in which there was no cloud-free imagery available in 1973 and instead report on the change between 1989 and 2022. **b**–**g**, Landsat image pairs showing examples of pinning-point evolution. The red arrows indicate pinning points that have reduced in area and the blue arrows indicate pinning points that have grown in area. Extensive examples of pinning-point mapping and animated images are located in the Supplementary Information. Landsat imagery courtesy of the US Geological Survey. Scale bars, 20 km (**b**,**e**), 10 km (**c**,**f**,**g**) and 5 km (**d**).

the dynamics of the entire Moscow University Glacier catchment. We observe more subtle losses of pinning at Totten Ice Shelf from 1973 to 1989 and 1989 to 2000, before more widespread pinning-point loss between 2000 and 2022 (Fig. 2). Outlet glaciers in Wilkes Land have been losing mass since the beginning of the satellite era[7]. Our results show that at least parts of their ice shelves were already thinning between 1973 and 1989. This hints that the initial trigger for mass loss and acceleration of outlet glaciers in Wilkes Land may have occurred pre-1973.

In Victoria Land and George V Land, we observe the loss of a major pinning point on the Campbell Glacier tongue and the shrinkage of a pinning point on the Rennick Ice Shelf in the 2000s, but limited change elsewhere (Fig. 2). The reduction in pinning of Rennick Ice Shelf is consistent with thinning in satellite altimetry[13] and, together with acceleration of the nearby Matusevich Glacier in the 2000s (refs. 7,35), implies that warm water has recently reached this part of the Victoria Land coastline. At Shackleton Ice Shelf, most pinning points have not experienced substantive change, but we do observe some variability in a band of pinning points near its ice front. There has, however, been major unpinning on the nearby Conger Ice Shelf following its gradual retreat since 1973. In Enderby Land, there was limited change in pinning at the Wilma-Robert-Downer Embayment and in Lützow-Holm Bay in 1973–1989 and 1989–2000, but a growth of pinning points in these regions between 2000 and 2022 (Extended Data Fig. 5) confirms that these ice shelves have thickened. In Lützow-Holm Bay, thickening is consistent with the strengthening of easterly winds reducing the inflow of warm water underneath ice shelves[38]. Further west, some pinning-point loss was experienced at the front of Roi Baudouin Ice Shelf, and a pinning point disappeared from neighbouring Borchgrevink Ice Shelf. In Dronning Maud and

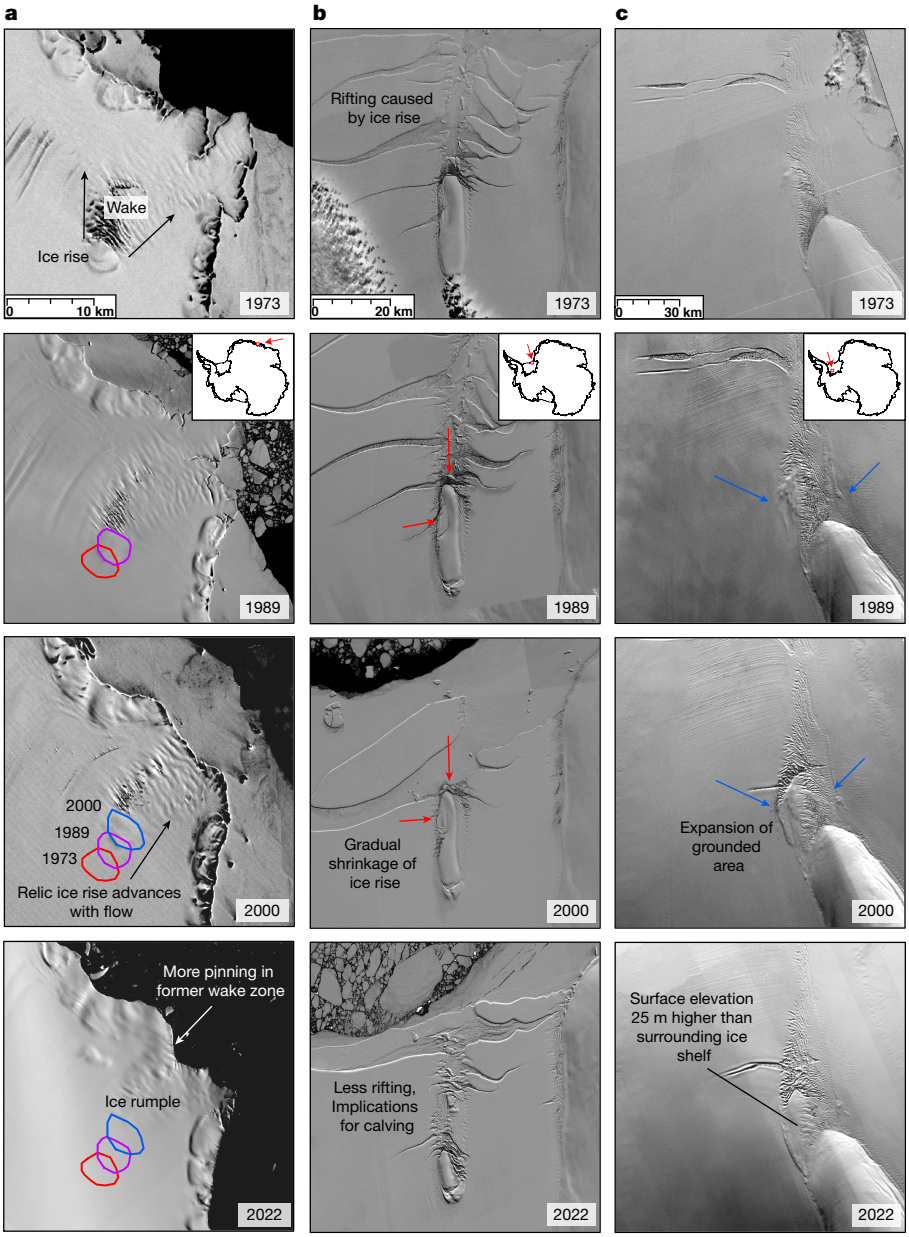

Fig. 4 | Examples of ice-rise evolution from five decades of Landsat imagery. **a**, Borchgrevink Ice Rise. **b**, Hemmen Ice Rise. **c**, Korff Ice Rise. Red arrows indicate areas in which the ice rise has shrunk, and blue arrows indicate areas in which the ice rise has grown. Landsat imagery courtesy of the US Geological Survey. Scale bars, 10 km (**a**), 20 km (**b**) and 30 km (**c**).

Coats Land, we observed very few changes to most of the pinning points that fringe the coastline. Across Filchner–Ronne Ice Shelf, most pinning points also remained unchanged over the past five decades, although there were some notable changes to some of the prominent ice rises.

Rapidly changing ice rises

The internal structures of ice rises have been crucial in reconstructing former ice-sheet flow and thickness change over centuries to millennia[39]. Some of our more striking observations are the particularly large breakups or growths of some ice rises, which provide insights into how these features evolve over decadal timescales. The 5-km-wide Borchgrevink Ice Rise ungrounded in the late 1970s (Fig. 4a), despite expressing limited ice-shelf thickness change in modern satellite-altimetry records[3,4]. This hints at vigorous ice-shelf thinning occurring before its ungrounding in the late 1970s, strongly implying that the sub-ice-shelf bathymetry is conducive to warm-water intrusions[40]. After ungrounding, the 'relic' ice rise was transported downstream through the 1990s and 2000s before regrounding towards the ice front and forming the present-day ice rumple (Fig. 4a). In 1973, Hemmen Ice Rise, located at the front of Ronne Ice Shelf, was 22 km along its long axis, whereafter for the following three decades it gradually shrank before breaking apart in the mid-2000s (Fig. 4b). Before this break-up, it had played an important part in regulating the calving of Ronne Ice Shelf by promoting rifting[22,23]. Today at this location, there is now less rifting, meaning a change in calving behaviour might be expected over the coming decades. At Korff Ice Rise, also located on Ronne Ice Shelf, we observe a 20-km growth of the grounded section of the ice rise on its northern flank (Fig. 4c). Analysis of the Reference Elevation Model of Antarctica (REMA) Digital Elevation Model[41] shows that the surface of this newly grounded section is now around 25 m higher than the

surrounding floating ice shelf. This may represent the first stages of expansion of the entire Korff Ice Rise. Importantly, current numerical models do not account for any feedback associated with major changes in ice rises. Our observations show that these processes can happen relatively rapidly and on sections of ice shelves in which there has been limited thickness change over the satellite-altimetry era.

Bleak future for some ice shelves

Our results have shown a marked, widespread and accelerating unanchoring of ice shelves from pinning points in the western Antarctic Peninsula and in the Amundsen Sea Sector over the past five decades (Fig. 3). Meanwhile, there has also been steady unanchoring of ice shelves from pinning points in the Wilkes Lands region of East Antarctica. The loss of many of these pinning points is likely to be permanent, owing to their hysteretic evolution[42], meaning that an ice-shelf thickening of a greater magnitude is required for pinning points to reform at comparable size. On multi-decadal timescales, this pinning-point loss may represent the first steps of irreversible ice-shelf loss and subsequent mass loss of the previously impounded ice sheet.

Our insight into the spatial pattern of ice-shelf thickness change in the 1970s and 1980s (Fig. 2) shows that ice-shelf thinning was already well underway in the Amundsen Sea Sector and Wilkes Land. After 1989, thinning has spread progressively across much of West Antarctica and the western Antarctic Peninsula, with previously unchanged pinning points reducing in extent through the 1990s to the present. We know that ice-shelf thinning is driven predominantly by warm modified Circumpolar Deep Water (MCDW) flooding the continental shelf and melting the bases of ice shelves[10,12]. However, the primary mechanism driving this progressive flooding of the continental shelf by warm MCDW over the past five decades remains unclear. There is some evidence that an anthropogenic-driven trend in winds over the continental-shelf edge in the Amundsen Sea may be driving an increase in MCDW transport onto the continental shelf since the 1920s (ref. 43). In East Antarctica, the poleward shift of MCDW since the 1930s in response to the poleward shift of westerly winds[44] may also be driving the thinning of ice shelves. Meanwhile, decadal-scale feedbacks emanating from the input of freshwater from ice-shelf melt onto the continental shelf may enhance the delivery of warm water beneath ice shelves on local scales[45], and the degree to which this may upscale to affect larger geographic scales continues to be investigated[46].

The overall acceleration of pinning-point loss is striking and paints a bleak future for many Antarctic ice shelves. From 2000 to 2022, the vast majority of pinning points in the 3,000-km stretch of coastline in West Antarctica from George VI Ice Shelf to Hull Glacier, along with an 800-km stretch of coastline in Wilkes Land, reduced in area or completely disappeared. Over the past 50 years, thinning at some of the most rapidly changing ice shelves means that they are close to being, or have already become, completely unanchored—for example, Thwaites Eastern Ice Shelf[47] and Pine Island Glacier[10]—which means that there is limited potential for further reductions in buttressing. Instead, the greatest concern may lie with those major ice shelves that are still substantially pinned but have shown clear signs of accelerated pinning-point loss. This includes George VI, Getz, Holmes, Moscow University and Totten ice shelves. A continuation of pinning-point loss in those locations will probably reduce buttressing and result in an acceleration in both ice discharge and mass loss.

Online content

Any methods, additional references, Nature Portfolio reporting summaries, source data, extended data, supplementary information, acknowledgements, peer review information; details of author contributions and competing interests; and statements of data and code availability are available at https://doi.org/10.1038/s41586-024-07049-0.

1. Greene, C. A., Gardner, A. S., Schlegel, N.-J. & Fraser, A. D. Antarctic calving loss rivals ice-shelf thinning. *Nature* **609**, 948–953 (2022).
2. Gudmundsson, G. H., Paolo, F. S., Adusumilli, S. & Fricker, H. A. Instantaneous Antarctic ice sheet mass loss driven by thinning ice shelves. *Geophys. Res. Lett.* **46**, 13903–13909 (2019).
3. Adusumilli, S., Fricker, H. A., Medley, B., Padman, L. & Siegfried, M. R. Interannual variations in meltwater input to the Southern Ocean from Antarctic ice shelves. *Nat. Geosci.* **13**, 616–620 (2020).
4. Hogg, A. E., Gilbert, L., Shepherd, A., Muir, A. S. & McMillan, M. Extending the record of Antarctic ice shelf thickness change, from 1992 to 2017. *Adv. Space Res.* **68**, 724–731 (2021).
5. Paolo, F. S., Fricker, H. A. & Padman, L. Volume loss from Antarctic ice shelves is accelerating. *Science* **348**, 327–331 (2015).
6. Matsuoka, K. et al. Antarctic ice rises and rumples: their properties and significance for ice-sheet dynamics and evolution. *Earth Sci. Rev.* **150**, 724–745 (2015).
7. Rignot, E. et al. Four decades of Antarctic ice sheet mass balance from 1979–2017. *Proc. Natl Acad. Sci. USA* **116**, 1095–1103 (2019).
8. The IMBIE team Mass balance of the Antarctic Ice Sheet from 1992 to 2017. *Nature* **558**, 219–222 (2018).
9. Glavovic, B. C. et al. in *Climate Change 2022: Impacts, Adaptation and Vulnerability*. Contribution of Working Group II to the Sixth Assessment Report of the Intergovernmental Panel on Climate Change (eds H.-O. Pörtner et al.) 2163–2194 (Cambridge Univ. Press, 2022).
10. Jenkins, A. et al. Observations beneath Pine Island Glacier in West Antarctica and implications for its retreat. *Nat. Geosci.* **3**, 468–472 (2010).
11. Jenkins, A. et al. West Antarctic Ice Sheet retreat in the Amundsen Sea driven by decadal oceanic variability. *Nat. Geosci.* **11**, 733–738 (2018).
12. Pritchard, H. D. et al. Antarctic ice-sheet loss driven by basal melting of ice shelves. *Nature* **484**, 502–505 (2012).
13. Smith, B. et al. Pervasive ice sheet mass loss reflects competing ocean and atmosphere processes. *Science* **368**, 1239–1242 (2020).
14. Adusumilli, S. et al. Variable basal melt rates of Antarctic Peninsula ice shelves, 1994–2016. *Geophys. Res. Lett.* **45**, 4086–4095 (2018).
15. Paolo, F. S. et al. Response of Pacific-sector Antarctic ice shelves to the El Niño/Southern Oscillation. *Nat. Geosci.* **11**, 121–126 (2018).
16. Edwards, T. L. et al. Revisiting Antarctic ice loss due to marine ice-cliff instability. *Nature* **566**, 58–64 (2019).
17. Ritz, C. et al. Potential sea-level rise from Antarctic ice-sheet instability constrained by observations. *Nature* **528**, 115–118 (2015).
18. Roberts, J. et al. Ocean forced variability of Totten Glacier mass loss. *Geol. Soc. Spec. Publ.* **461**, 175–186 (2018).
19. Favier, L., Pattyn, F., Berger, S. & Drews, R. Dynamic influence of pinning points on marine ice-sheet stability: a numerical study in Dronning Maud Land, East Antarctica. *Cryosphere* **10**, 2623–2635 (2016).
20. Fürst, J. J. et al. The safety band of Antarctic ice shelves. *Nat. Clim. Change* **6**, 479–482 (2016).
21. Reese, R., Gudmundsson, G. H., Levermann, A. & Winkelmann, R. The far reach of ice-shelf thinning in Antarctica. *Nat. Clim. Change* **8**, 53–57 (2018).
22. Larour, E., Rignot, E. & Aubry, D. Modelling of rift propagation on Ronne Ice Shelf, Antarctica, and sensitivity to climate change. *Geophys. Res. Lett.* **31**, L16404 (2004).
23. Rignot, E. & MacAyeal, D. R. Ice-shelf dynamics near the front of the Filchner—Ronne Ice Shelf, Antarctica, revealed by SAR interferometry. *J. Glaciol.* **44**, 405–418 (1998).
24. Holland, P. R., Bevan, S. L. & Luckman, A. J. Strong ocean melting feedback during the recent retreat of Thwaites Glacier. *Geophys. Res. Lett.* **50**, e2023GL103088 (2023).
25. Bindschadler, R. et al. The Landsat Image Mosaic of Antarctica. *Remote Sens. Environ.* **112**, 4214–4226 (2008).
26. Cook, A. J. & Vaughan, D. G. Overview of areal changes of the ice shelves on the Antarctic Peninsula over the past 50 years. *Cryosphere* **4**, 77–98 (2010).
27. Mitcham, T., Gudmundsson, G. H. & Bamber, J. L. The instantaneous impact of calving and thinning on the Larsen C Ice Shelf. *Cryosphere* **16**, 883–901 (2022).
28. Padman, L. et al. Oceanic controls on the mass balance of Wilkins Ice Shelf, Antarctica. *J. Geophys. Res.* **117**, C01010 (2012).
29. Cochran, J. R., Jacobs, S. S., Tinto, K. J. & Bell, R. E. Bathymetric and oceanic controls on Abbot Ice Shelf thickness and stability. *Cryosphere* **8**, 877–889 (2014).
30. Hogg, A. E. et al. Increased ice flow in Western Palmer Land linked to ocean melting. *Geophys. Res. Lett.* **44**, 4159–4167 (2017).
31. Christie, F. D. W., Bingham, R. G., Gourmelen, N., Tett, S. F. B. & Muto, A. Four-decade record of pervasive grounding line retreat along the Bellingshausen margin of West Antarctica. *Geophys. Res. Lett.* **43**, 5741–5749 (2016).
32. Oelerich, R., Heywood, K. J., Damerell, G. M. & Thompson, A. F. Wind-induced variability of warm water on the southern Bellingshausen Sea continental shelf. *J. Geophys. Res. Oceans* **127**, e2022JC018636 (2022).
33. Smith, J. A. et al. Sub-ice-shelf sediments record history of twentieth-century retreat of Pine Island Glacier. *Nature* **541**, 77–80 (2017).
34. Graham, A. G. C. et al. Rapid retreat of Thwaites Glacier in the pre-satellite era. *Nat. Geosci.* **15**, 706–713 (2022).
35. Miles, B. W. J. et al. High spatial and temporal variability in Antarctic ice discharge linked to ice shelf buttressing and bed geometry. *Sci. Rep.* **12**, 10968 (2022).
36. Campbell, A. J., Hulbe, C. L. & Lee, C.-K. Ice stream slowdown will drive long-term thinning of the Ross Ice Shelf, with or without ocean warming. *Geophys. Res. Lett.* **45**, 201–206 (2018).
37. Bindschadler, R. & Vornberger, P. Changes in the West Antarctic Ice Sheet since 1963 from declassified satellite photography. *Science* **279**, 689–692 (1998).
38. Miles, B. W. J. et al. Slowdown of Shirase Glacier, East Antarctica, caused by strengthening alongshore winds. *Cryosphere* **17**, 445–456 (2023).
39. Wearing, M. G. & Kingslake, J. Holocene formation of Henry Ice Rise, West Antarctica, inferred from ice-penetrating radar. *J. Geophys. Res. Earth Surf.* **124**, 2224–2240 (2019).

40. Eisermann, H., Eagles, G., Ruppel, A. S., Läufer, A. & Jokat, W. Bathymetric control on Borchgrevink and Roi Baudouin ice shelves in East Antarctica. *J. Geophys. Res. Earth Surf.* **126**, e2021JF006342 (2021).
41. Howat, I. M., Porter, C., Smith, B. E., Noh, M.-J. & Morin, P. The Reference Elevation Model of Antarctica. *Cryosphere* **13**, 665–674 (2019).
42. Henry, A. C. J., Drews, R., Schannwell, C. & Višnjević, V. Hysteretic evolution of ice rises and ice rumples in response to variations in sea level. *Cryosphere* **16**, 3889–3905 (2022).
43. Holland, P. R., Bracegirdle, T. J., Dutrieux, P., Jenkins, A. & Steig, E. J. West Antarctic ice loss influenced by internal climate variability and anthropogenic forcing. *Nat. Geosci.* **12**, 718–724 (2019).
44. Herraiz-Borreguero, L. & Naveira Garabato, A. C. Poleward shift of Circumpolar Deep Water threatens the East Antarctic Ice Sheet. *Nat. Clim. Change* **12**, 728–734 (2022).
45. Silvano, A. et al. Freshening by glacial meltwater enhances melting of ice shelves and reduces formation of Antarctic Bottom Water. *Sci. Adv.* **4**, eaap9467 (2018).
46. Flexas, M. M., Thompson, A. F., Schodlok, M. P., Zhang, H. & Speer, K. Antarctic Peninsula warming triggers enhanced basal melt rates throughout West Antarctica. *Sci. Adv.* **8**, eabj9134 (2022).
47. Gudmundsson, G. H., Barnes, J. M., Goldberg, D. N. & Morlighem, M. Limited impact of Thwaites Ice Shelf on future ice loss from Antarctica. *Geophys. Res. Lett.* **50**, e2023GL102880 (2023).

Methods

Satellite imagery

We used the Landsat-1 and Landsat-2 satellite-image archive to create the earliest near-cloud-free mosaic of the ice shelves of Antarctica from the 1970s. Each image incorporated into the mosaic has a spatial resolution of 60 m. From a preliminary inspection of the imagery, Band 4 was determined to be the most suitable for pinning-point identification. There are relatively few repeat Landsat-1 and Landsat-2 image scenes and each footprint often had only a small handful of available images. Therefore, we downloaded all available images, including images with high cloud-cover percentages, because some still contained valuable cloud-free sections of ice shelves. The geolocation accuracy of the Landsat-1 and Landsat-2 imagery in Antarctica is poor and images were often offset by 10 s of kilometres. Therefore, we manually co-registered each image by tying stable features (for example, exposed bedrock or buried features in the grounded ice) to Landsat-8 and Landsat-9 imagery, which have excellent geolocation accuracy. For most Landsat-1 and Landsat-2 images, this gave co-registration accuracy to within 2 pixels. However, for a minority of images with few or no exposed bedrock, the co-registration accuracy may be greater than this. By filtering through all co-registered images and selecting the optimum cloud-free combination of imagery, we were able to produce a near-cloud-free mosaic covering nearly all ice shelves of Antarctica (Extended Data Fig. 2). The main exception to this is in the northern Antarctic Peninsula, in which there were no cloud-free images available over Larsen and Prince Gustav ice shelves. Elsewhere, the gaps were small and isolated. The mosaic consists of 251 images: 15% are from 1972, 59% from 1973, 19% from 1974, 6% from 1975, 1% from 1976 and less than 1% from 1978. For this paper, we ascribe to the mosaic a year stamp of 1973. A full list of the images used is available in Supplementary Table 1.

We undertook a similar process for the late 1980s ('1989') mosaic using Landsat-4 and Landsat-5 imagery. We used Band 2 to be consistent with the wavelength of Band 4 in the Landsat-1 and Landsat-2 satellites, and each image has a spatial resolution of 30 m. The geolocation accuracy of these images is also poor and required manual co-registration with the raw imagery offset by 100 s of metres. The optimum cloud-free combination of imagery provided complete coverage of all ice shelves apart from small isolated regions of cloud cover and the extreme southern sections of Filchner–Ronne and Ross ice shelves (Extended Data Fig. 1). The mosaic consists of 297 images: 8% are from 1986, 2% from 1987, 12% from 1988, 54% from 1989, 22% from 1990 and 2% from 1991. For the purposes of this paper, we ascribe a year stamp of 1989 to the mosaic. A full list of the images used is available in Supplementary Table 1.

For 2000, we used the Landsat Image Mosaic of Antarctica (LIMA)[25], which consists of cloud-free Landsat-7 imagery spanning 1999–2003 with a spatial resolution of 30 m. For 2022, we create a mosaic using Google Earth Engine[48]. We simply selected the most recent Landsat-8 or Landsat-9 imagery with cloud cover of less than 5%, with the earliest date of 1 January 2021. For the few regions in which cloud cover remained, we manually selected cloud-free Landsat-8 or Landsat-9 imagery to cover the small gaps. We used Band 3 to be consistent with earlier imagery that has a spatial resolution of 30 m.

Pinning-point mapping

We primarily identified pinning-point locations using an existing inventory of ice rise and rumples[6,49]. Moreover, we used the MEaSUREs interferometry grounding-line product[50,51] to detect pinning points that were not included in reference[6]. We also manually identified several pinning points that were not included in either the ice rise and rumple dataset or the MEaSUREs product, and some pinning points that were present in the 1970s but have subsequently unpinned.

Each pinning point forms a bump on the otherwise smooth ice-shelf surface that is typically visible in optical imagery. The surface expression of this bump changes through time as an ice-shelf thickens or thins[10,18], in response to its altering proportion of contact with the underlying bedrock high (Fig. 1). For each of our epochs, we classified the change in the surface expression of each pinning point into three categories: growing in area, reducing in area or no detectable change. If a pinning point disappeared between two sets of images, we recorded it as reducing in area. We classified pinning-point change directly from each Landsat scene by magnifying each pinning point and finding the optimum contrast, before flicking between each successive epoch. For 1973 and 1989, there was often only one available cloud-free image over each ice shelf, making it impossible to be consistent in terms of choosing Landsat images with similar solar azimuth angles. In a small number of cases, extremes in lighting caused by differing solar zenith angles between mosaics may have had an impact on our classification of pinning-point change. In the small number of cases in which it is unclear if the surface expression of pinning points has changed, or if it simply reflects a change in atmospheric conditions (for example, shadows) or an artefact of comparing imagery of different qualities, we erred on the side of caution and classified them as showing no detectable change. However, for the vast majority of pinning points, the direction of change is obvious between the periods over which we examined change, and we include detailed examples of our classifications from every major ice shelf in Supplementary Fig. 1 and through animated imagery. Even for those images that were offset by greater than two Landsat-1 pixels (> 120 m) the change in shape of pinning points is clear.

Comparison with satellite altimetry

We compared our pinning-point classification results with satellite-altimetry-based observations of ice-shelf thickness change over the overlapping time period. The longest available time series of satellite-altimetry-derived ice-shelf thickness change stretches from 1992 to 2018 (ref. 3), but this dataset is relatively coarse, with a spatial resolution of 10 km, and its coverage of some of the smaller ice shelves is limited. Instead we focus our comparison on the ice-shelf thickness change dataset derived from the ICESat and ICESat-2 satellites between 2003 and 2019 (ref. 13). This dataset has a higher spatial resolution (5 km), covers all floating ice shelves, and its timespan is a very close match to our 2000–2022 epoch of pinning-point change (Extended Data Fig. 2). We extracted the median thickness change from a 7.5-km buffer surrounding each pinning point in which there is available data (n = 467). The median thickness change is compared with the mapped direction of change for each pinning point. Overall 86% of pinning points that grew in size correspond to regions of ice-shelf thickening (>0 m yr^{-1}), 66% of pinning points that reduced in extent correspond to regions of ice-shelf thinning (<0 m yr^{-1}) and 85% of the pinning points that did not change notably in area correspond to regions of limited change in ice-shelf thickness classified as between −1 m yr^{-1} and 1 m yr^{-1} (Extended Data Fig. 3). The main reason why we do not detect change in some pinning points while the surrounding floating ice thins is related to the underlying topography beneath pinning points. A pinning point resting on flat topography would require relatively small reductions in ice-shelf thickness for ice to unground from a large surface area, resulting in large visual changes at the surface from optical imagery. This is in contrast to a pinning point with steep sides, in which relatively small reductions in ice-shelf thickness may cause only a very small area of the pinning point to unground, resulting in very small changes to the pinning-point area at the surface, that are not detectable in Landsat imagery.

Data availability

All Landsat data used in this study are freely available to download from USGS Earth Explorer, and we include a list of all scenes used in the Supplementary Information. The co-registered Landsat scenes used

in the 1973 and 1989 mosaics[52] are available to download from https://doi.org/10.7488/ds/3810. The 2022 Landsat mosaic[53] is available to download from https://doi.org/10.7488/ds/7531. The shapefiles that map the direction of pinning-point change are available in the Supplementary Information and at https://doi.org/10.7488/ds/7583 (ref. 54). The inventory of ice rises and rumples[43] used to locate pinning points is available at https://doi.org/10.21334/npolar.2015.9174e644. The MEaSUREs Antarctic Grounding Line from Differential Satellite Radar Interferometry[44] is available at https://doi.org/10.5067/IKBWW4RYHF1Q. All mapping figures were produced using ArcMap 10.8.

48. Gorelick, N. et al. Google Earth Engine: planetary-scale geospatial analysis for everyone. *Remote Sens. Environ.* **202**, 18–27 (2017).
49. Moholdt, G. & Matsuoka, K. Inventory of Antarctic ice rises and rumples (version 1). Norwegian Polar Institute https://doi.org/10.21334/npolar.2015.9174e644 (2015).
50. Rignot, E., Mouginot, J. & Scheuchl, B. MEaSUREs Antarctic Grounding Line from Differential Satellite Radar Interferometry, Version 2. NASA National Snow and Ice Data Center Distributed Active Archive Center https://doi.org/10.5067/IKBWW4RYHF1Q (2016).
51. Rignot, E., Mouginot, J. & Scheuchl, B. Antarctic grounding line mapping from differential satellite radar interferometry. *Geophys. Res. Lett.* **38**, L10504 (2011).
52. Miles, B. & Bingham, R. Landsat mosaics of Antarctic Ice Shelves from 1973 and 1989, 1973-1989. Univ. Edinburgh, School of Geosciences https://doi.org/10.7488/ds/3810 (2023).
53. Miles, B. & Bingham, R. Landsat mosaics of Antarctic Ice Shelves from 2022 [dataset]. Univ. Edinburgh, School of Geosciences https://doi.org/10.7488/ds/7531 (2023).
54. Miles, B. & Bingham, R. Antarctic ice shelf pinning point change classification 1973-2022. Univ. Edinburgh, School of Geosciences https://doi.org/10.7488/ds/7583 (2023).

Acknowledgements Landsat imagery was provided free of charge by the US Geological Survey Earth Resources Observation Science Center. B.W.J.M. was supported by a Leverhulme Early Career Fellowship (ECF-2021-484). R.G.B. acknowledges funding from the UK Natural Environment Research Council (NE/S006613/1). We thank A. Jenkins for providing the normalized ocean temperature index for the Amundsen Sea.

Author contributions B.W.J.M. and R.G.B. conceived the study. B.W.J.M. processed the satellite imagery, generated the 1973 and 1989 mosaics and mapped the pinning-point changes. Both authors analysed and interpreted the results. B.W.J.M. produced all the figures and wrote the paper, with contributions from R.G.B.

Competing interests The authors declare no competing interests.

Additional information

Supplementary information The online version contains supplementary material available at https://doi.org/10.1038/s41586-024-07049-0.

Correspondence and requests for materials should be addressed to Bertie W. J. Miles.

Peer review information *Nature* thanks Catherine Walker and the other, anonymous, reviewer(s) for their contribution to the peer review of this work. Peer reviewer reports are available.

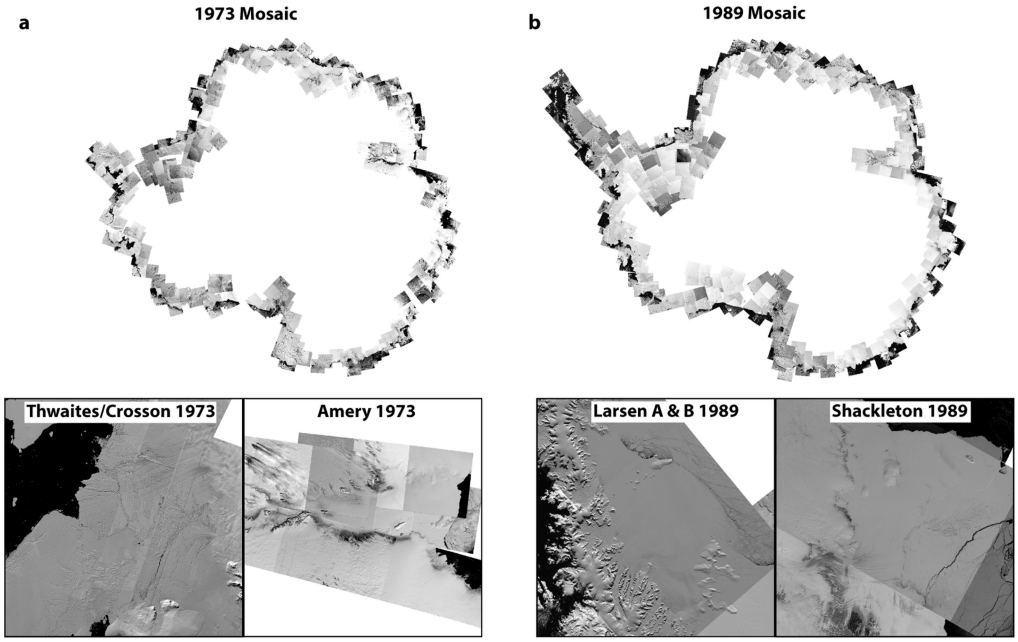

Extended Data Fig. 1 | Mosaics of Antarctic ice shelves. a) 1973 Landsat-1/Landsat-2 mosaic with example imagery from Thwaites Glacier/Crosson Ice Shelf and Amery Ice Shelf. **b)** 1989 Landsat-4 / Landsat-5 mosaic with example imagery from Larsen A and B Ice Shelves, along with Shackleton Ice Shelf. Landsat imagery courtesy of the U.S. Geological Survey.

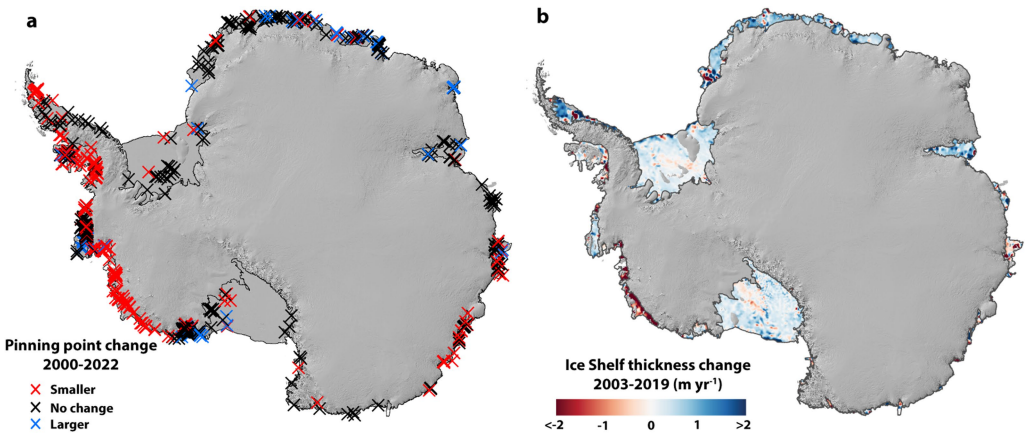

Extended Data Fig. 2 | Comparison between mapped pinning point change and altimetry derived ice shelf thickness change. a) mapped pinning-point change from 2000-2022 (this study) and **b)** ICESat derived ice-shelf thickness change from 2003-2019[13]. Note the broad agreement in the spatial pattern of change. In both panels data is overlain on the REMA mosaic of Antarctica[41].

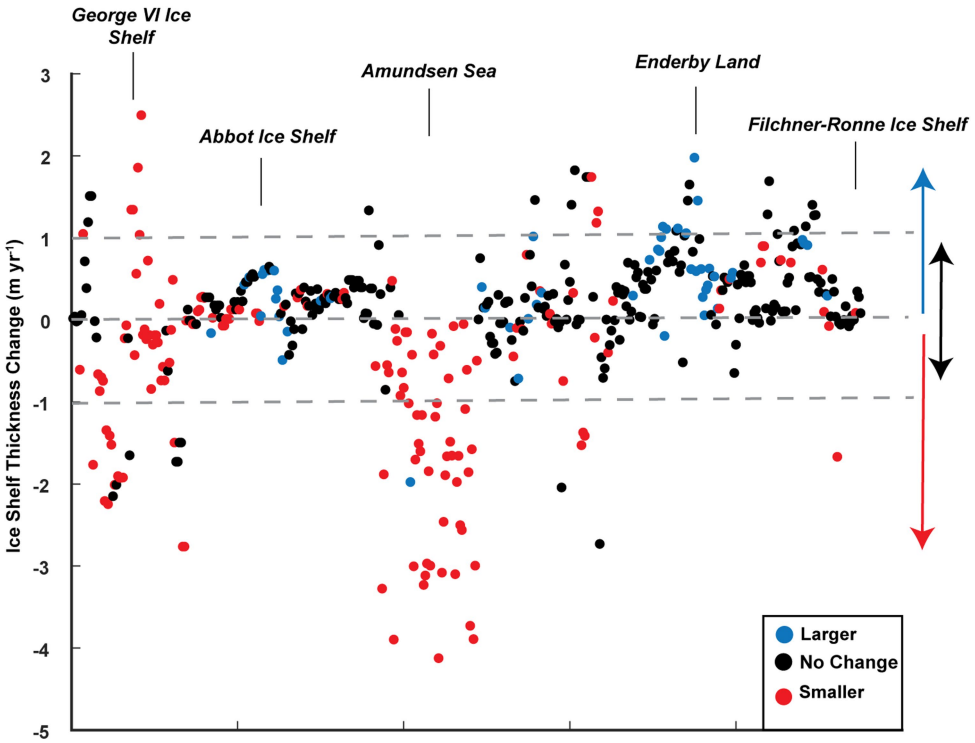

Extended Data Fig. 3 | Comparison between ice-shelf thickness change and pinning points. Satellite altimetry derived ice-shelf thickness change extracted from the vicinity of pinning points 2003–2019[13], with each data point colour coded in relation to mapped pinning point change 2000–2022. Data points are plotted from east to west, starting at the Antarctic Peninsula. The blue arrow on the right represents the quadrant for thickening (>0 m yr^{-1}), where 86% of growing pinning points are located (blue dots). The black arrows on the right represent the quadrant for limited thickness change (between −1 and 1 m yr^{-1}), where 85% of the pinning points that are not changing in size (black dots) are located. The red arrow on the right represents the quadrant for ice shelf thinning (<0 m yr^{-1}), where 66% of the pinning points that are reducing in size (red dots) are located.

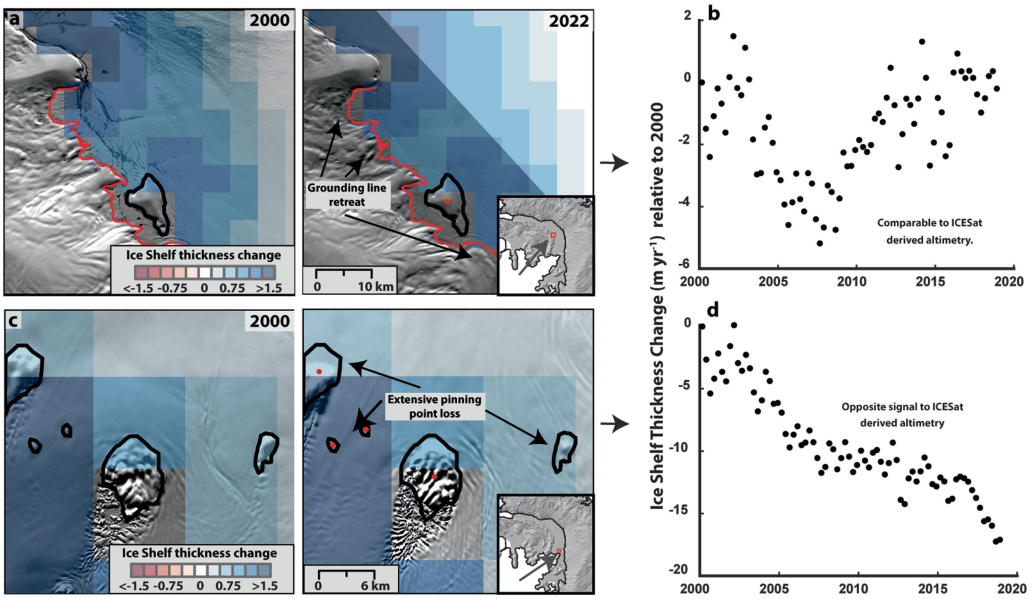

Extended Data Fig. 4 | Examples of mismatches between pinning point mapping and ice shelf thickness change from satellite altimetry. a) Ice-shelf thickness change between 2003 and 2019[13] from ICESat laser altimetry overlain on pinning-point change between 2000 and 2022 for Martin Ice Rise, George VI Ice Shelf. **b)** Time series of radar altimetry derived ice-shelf thickness change[3] averaged over the area shown in a and b. Satellite-altimetry products show thickening or limited change, but grounding-line retreat and extensive pinning-point loss identified here from the Landsat imagery suggest localised thinning. **c)** Same as a and b, but located over a cluster of pinning points at the southern ice front of George VI Ice Shelf. **d)** Time series of radar altimetry derived ice-shelf thickness change[3] averaged over area shown in d and e. Satellite-altimetry products differ over this area in terms of direction of ice-shelf thickness change.

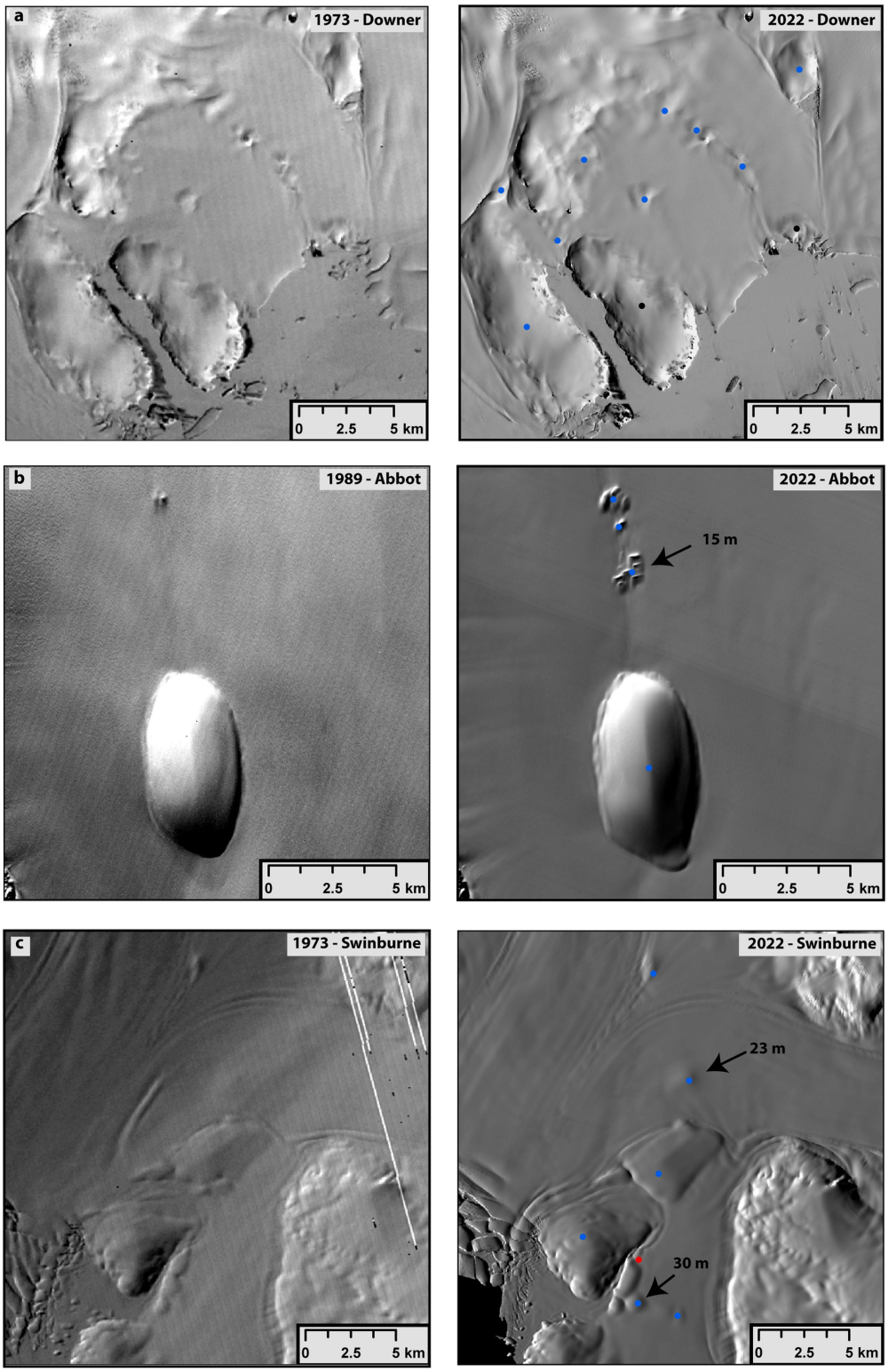

Extended Data Fig. 5 | Examples of pinning-point growth from pairs of Landsat satellite images. a) Wilma-Robert-Downer Glacier system, **b)** Abbot Ice Shelf and **c)** Swinburne Ice Shelf, with pinning-point change mapping overlain as small circles (coloured blue for growth, red for shrinkage). The numbers represent the difference in surface elevation between the pinning point and the surrounding flat ice shelf derived from the REMA DEM[41]. At these locations, this represents the minimum amount of ice-shelf thickening. Extensive examples of pinning-point mapping and animated images are located in the Supplementary Information. Landsat imagery courtesy of the U.S. Geological Survey.

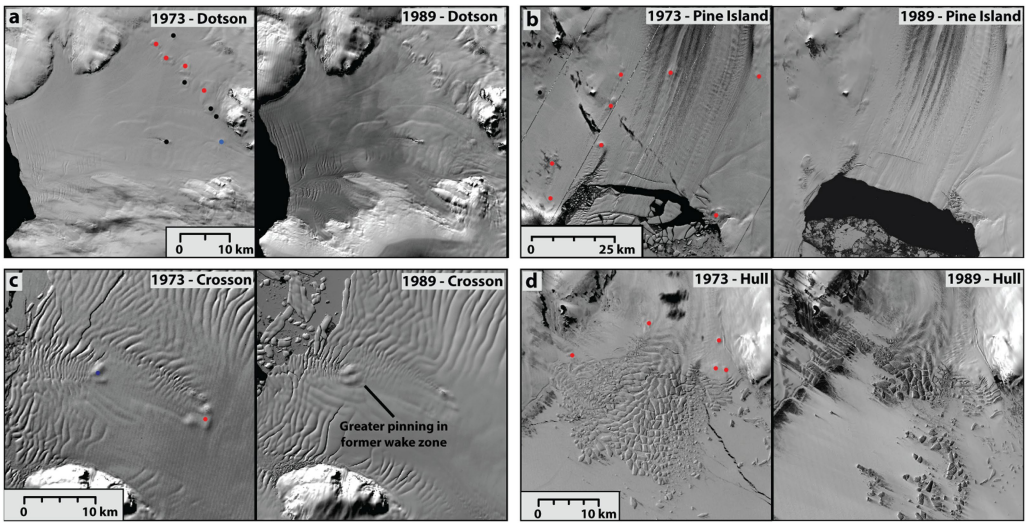

Extended Data Fig. 6 | Examples of pinning-point change in West Antarctica between 1973 and 1989. a) Dotson Ice Shelf, **b)** Pine Island Glacier Ice Shelf, **c)** Crosson Ice Shelf, **d)** Hull Glacier. Small circles mark pinning points mapped for this study (coloured red for shrinkage, blue for growth). Landsat imagery courtesy of the U.S. Geological Survey.

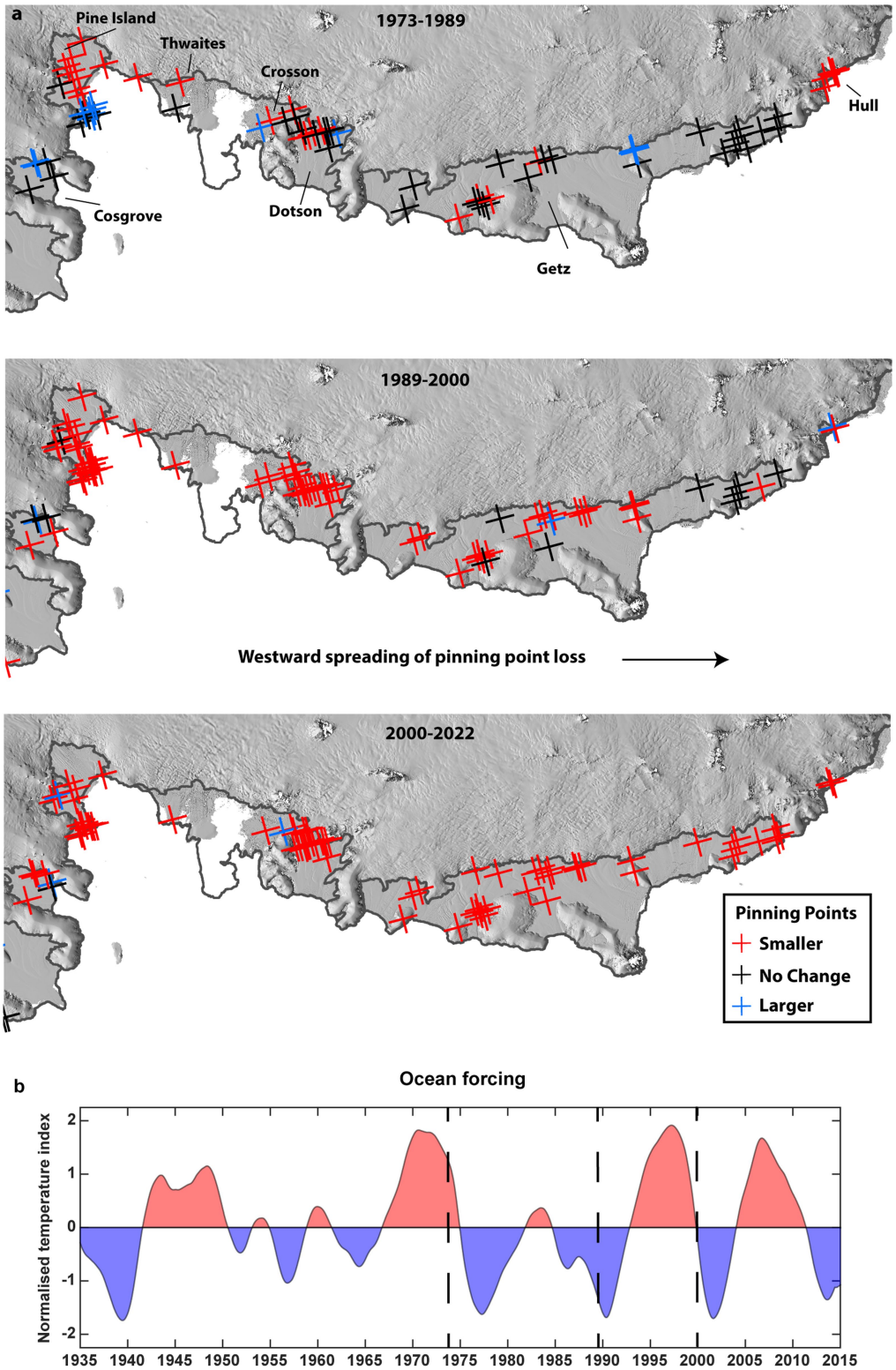

Extended Data Fig. 7 | Pinning-point change in the Amundsen Sea Sector over the past five decades and ocean forcing reconstructions. a) Mapped pinning point from 1973–1989, 1989–2000 and 2000–2022 overlain on the REMA mosaic[41]. Pinning-point loss spread westward over the past five decades. **b)** Normalized ocean-temperature index for the eastern Amundsen Sea inferred from central tropical Pacific sea-surface temperatures[11]. Dotted lines represent the epoch boundaries in this study. The period 1973–1989 is characterised by relatively cool ocean forcing.

Supplementary Information

Examples of pinning point change. The multi panel figure shows Landsat imagery from 1973, 1989, 2000 and 2022 over a selection of 108 pinning points. Mapping of pinning point change is overlain. Black crosses represent no change, red crosses represent a reduction in pinning point size and blue crosses represent an increase in size. The location of each pinning point and name, where available, is included in each heading. The ID number is the identification number provided in Matsuoka et al. (2015) pinning point database, pinning points that were not included in the Matsuoka et al. database are labelled as 'ID N/A'.

Landsat scenes used to create mosaics. A list of all Landsat scene ID's used in 1973 and 1989 mosaics of Antarctic ice shelves.

Supplementary Data: Animated images of pinning point change. A series of animated imagery flicking between 1973, 1989, 2000 and 2022 over key ice shelves and pinning points.

Larsen D - Buttler Island - ID 625

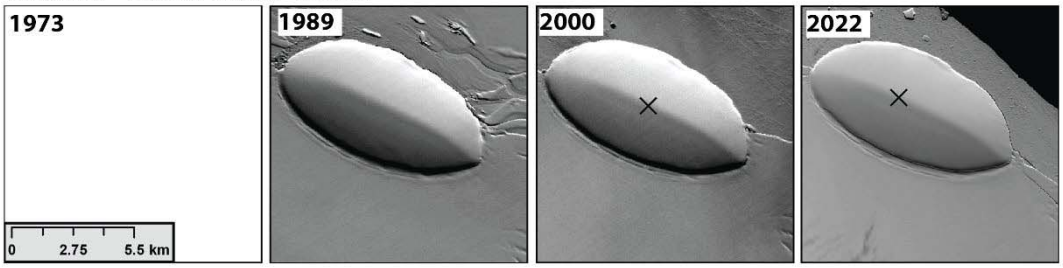

Larsen C- ID N/A

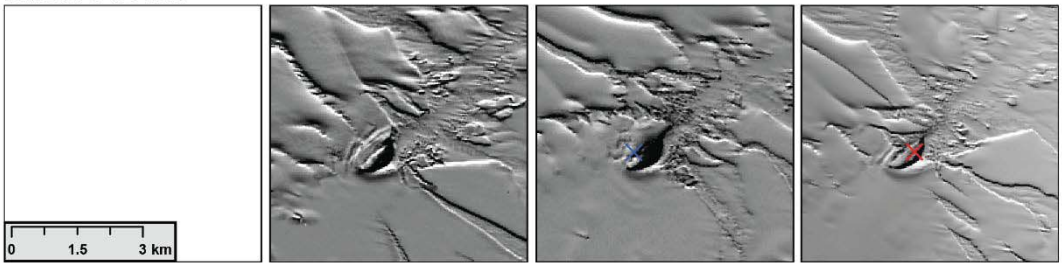

Larsen C - Bawden Ice Rise - ID 626

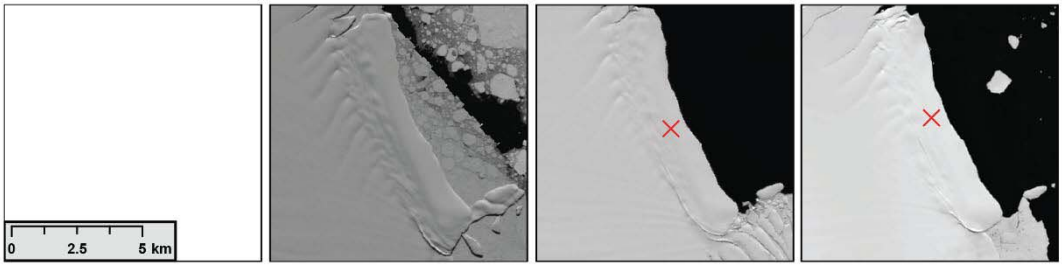

Larsen C - Tonkin Island - ID 588

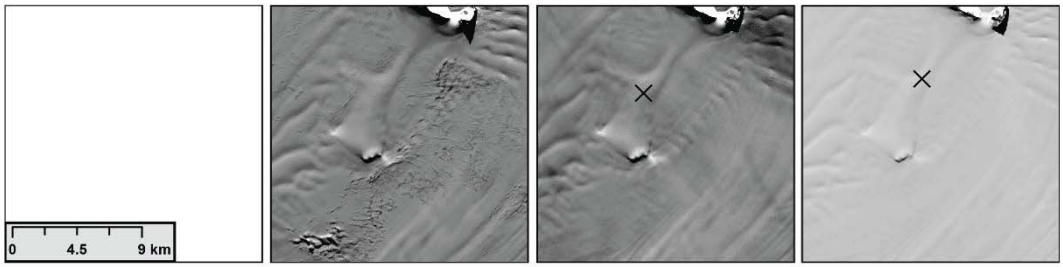

Larsen C - ID 599

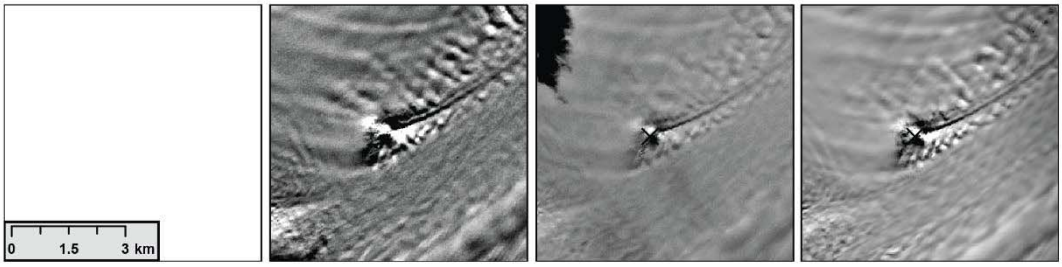

Larsen B - ID 613-632

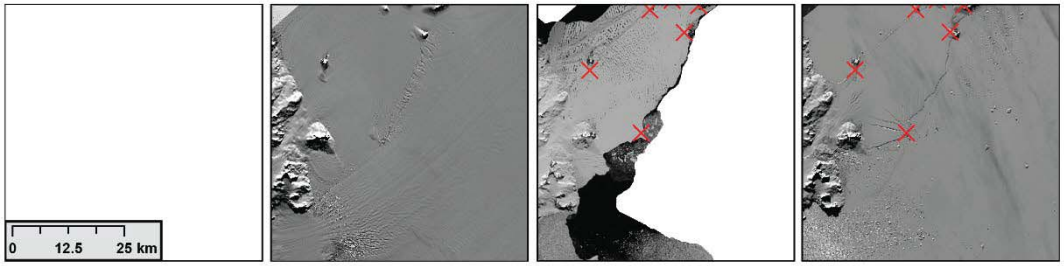

Prince Gustav - ID N/A

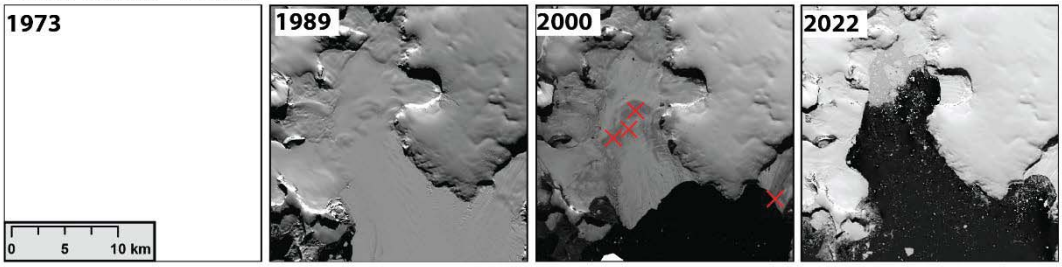

Wordie- ID 577

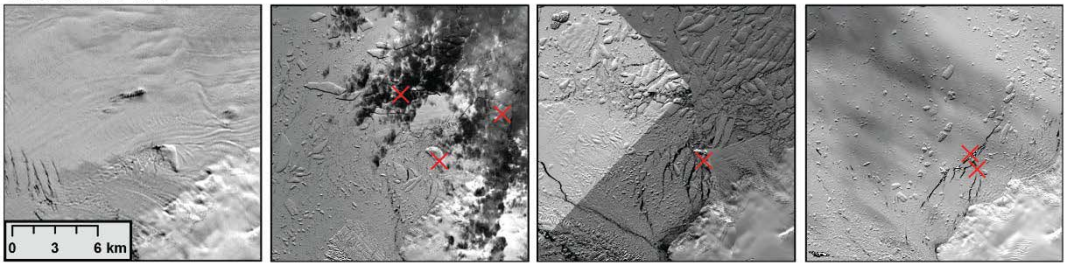

Wilkins - Petrie Ice Rises - ID 506

Wilkins - ID 524-528

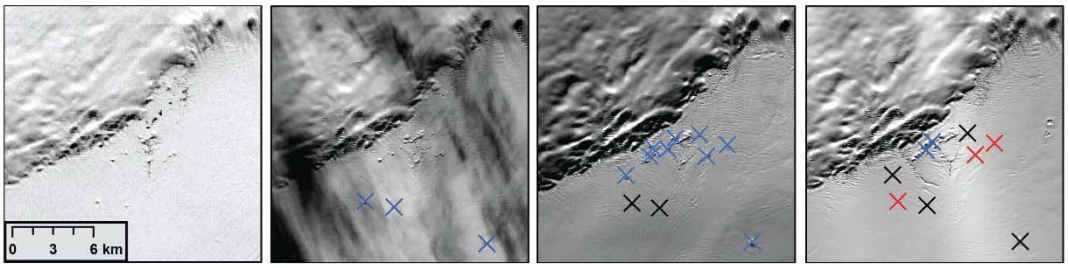

Bach - ID 487

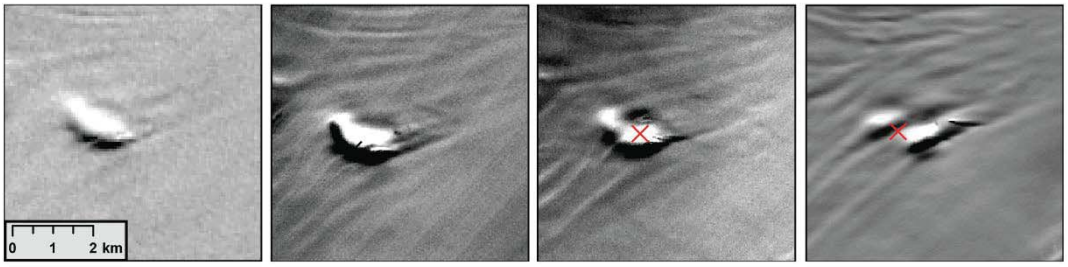

Bach- ID 557-560

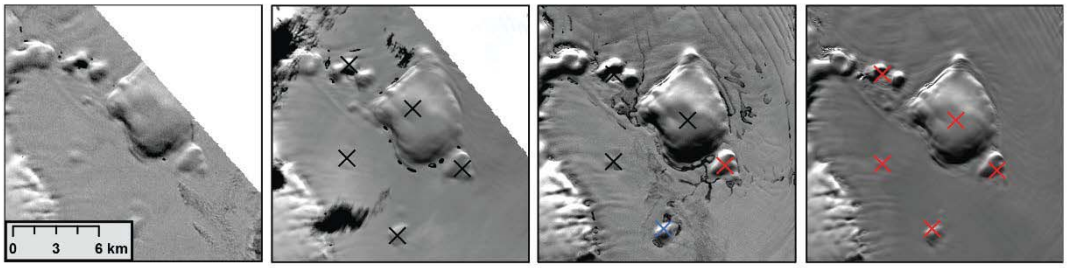

George VI - Martin Ice Rise - ID 572

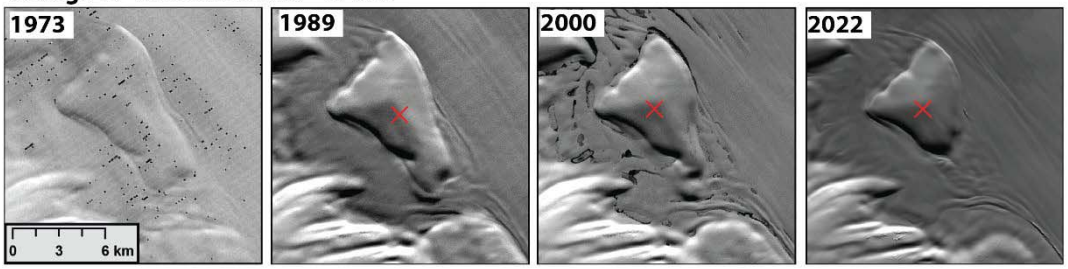

George VI - ID 581

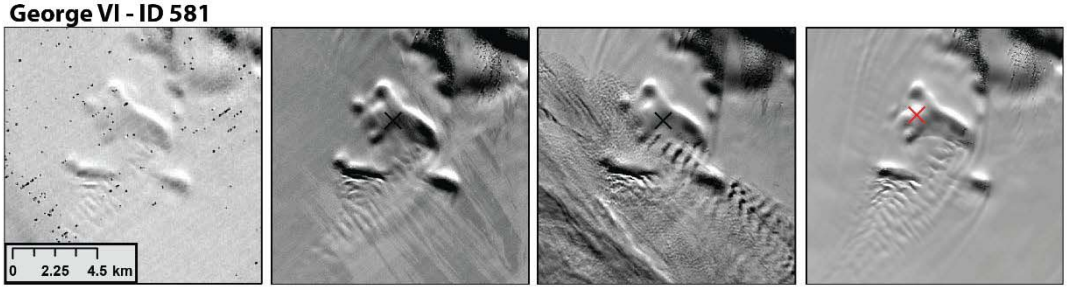

Stange - ID 468

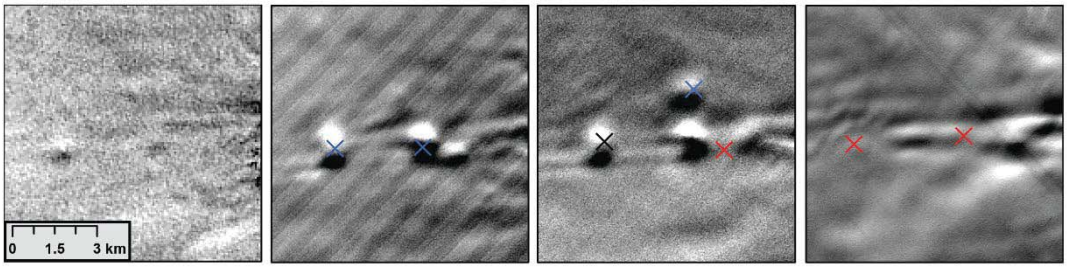

Stange- ID 485

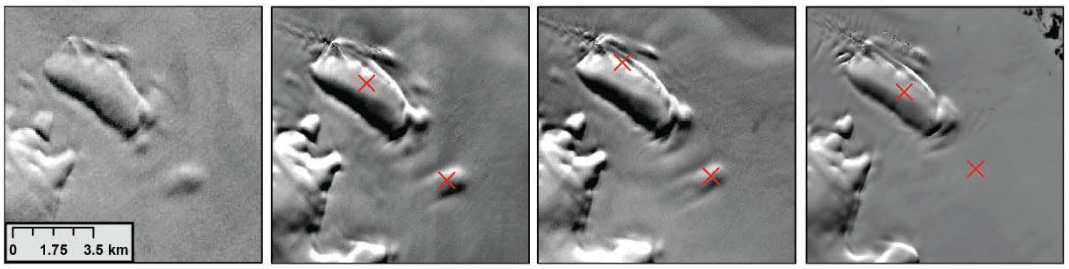

Venable- ID 457

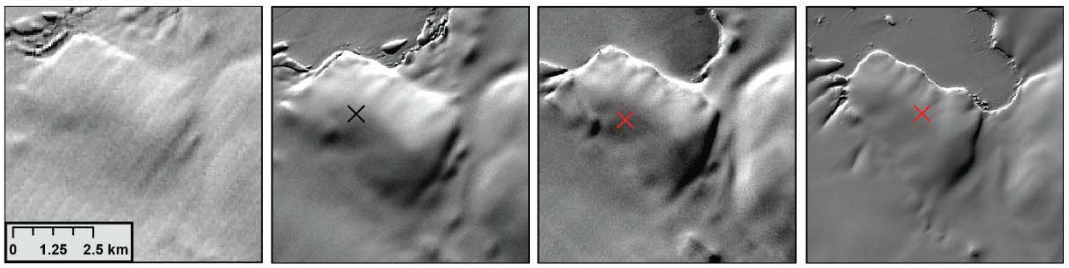

Venable- ID 459

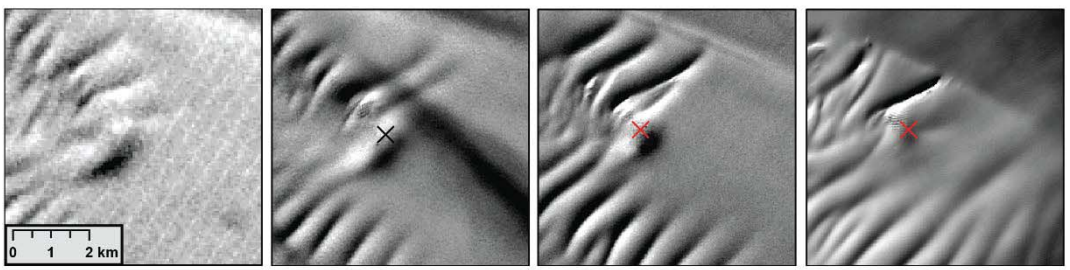

Venable- ID 460

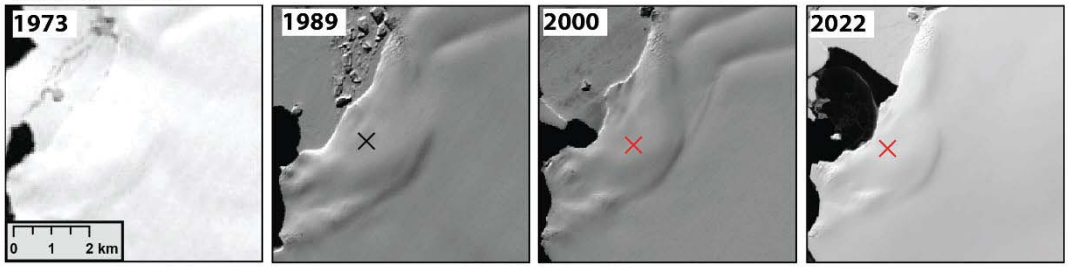

Abbot- ID N/A

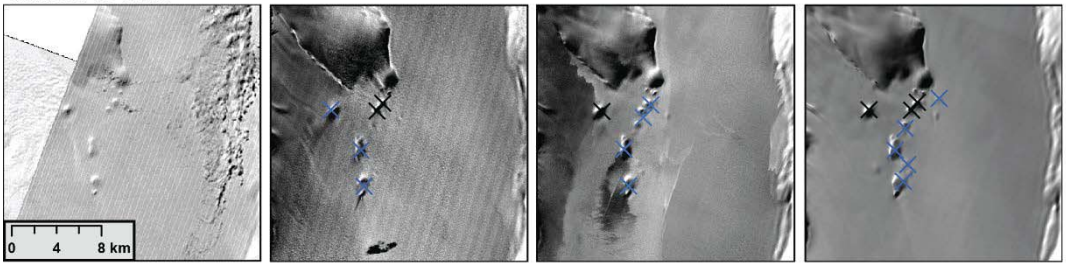

Abbot- ID 424

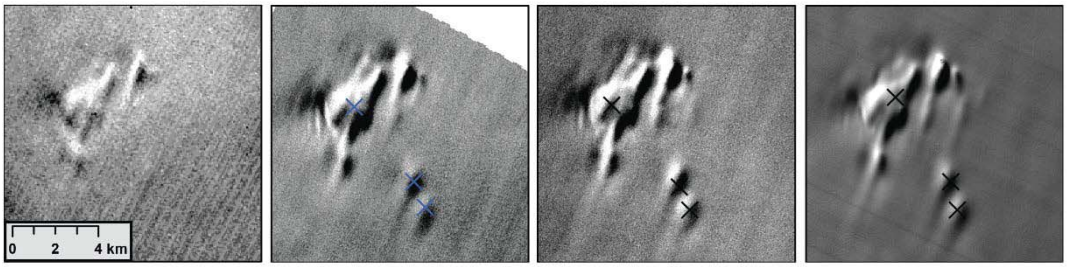

Abbot- ID 427-435

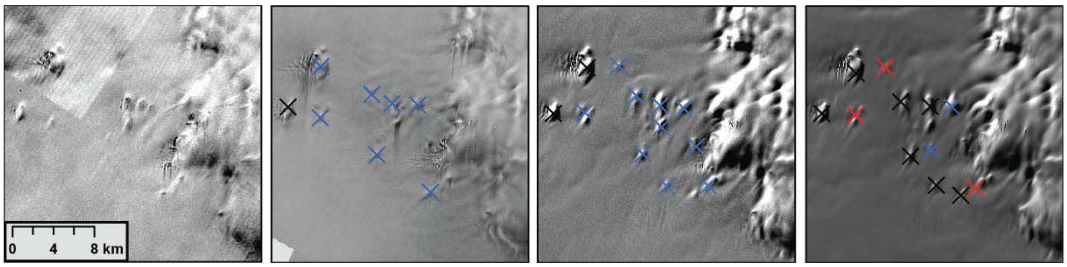

Abbot- ID 441

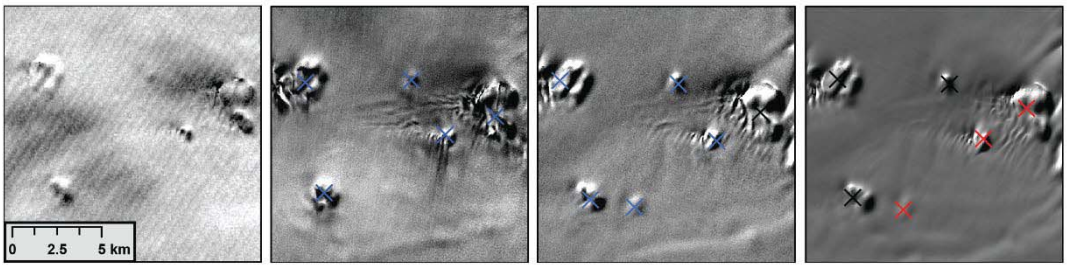

Crosgrove- ID 388-389

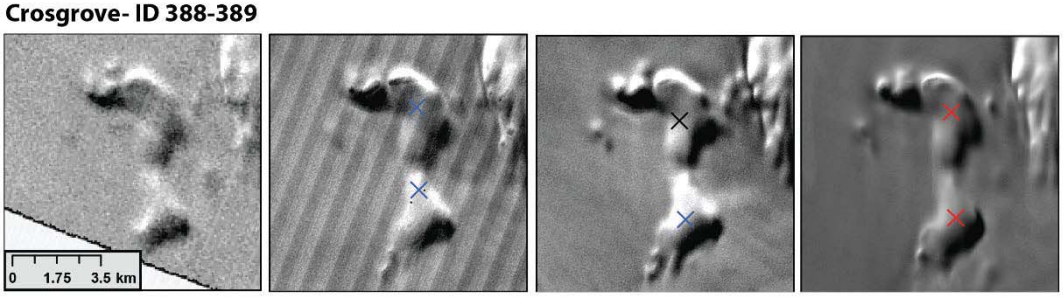

Crosgrove- ID N/A

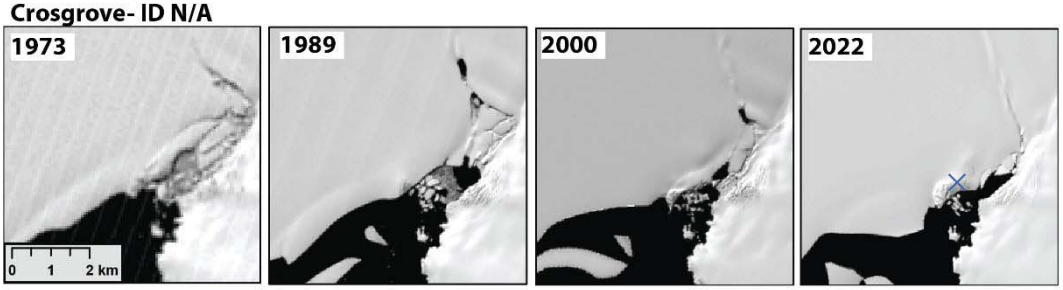

Pine Island- ID N/A

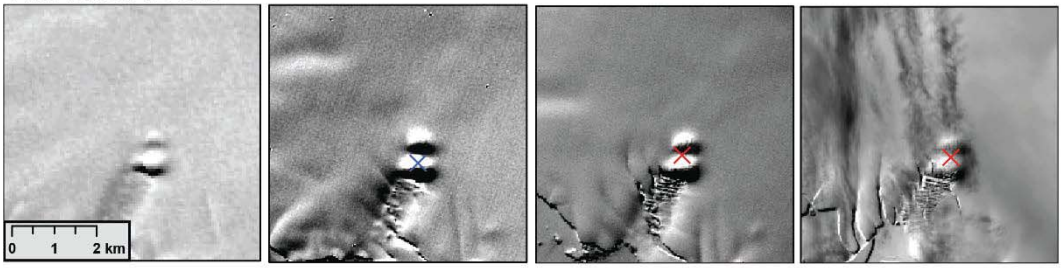

Pine Island- ID N/A

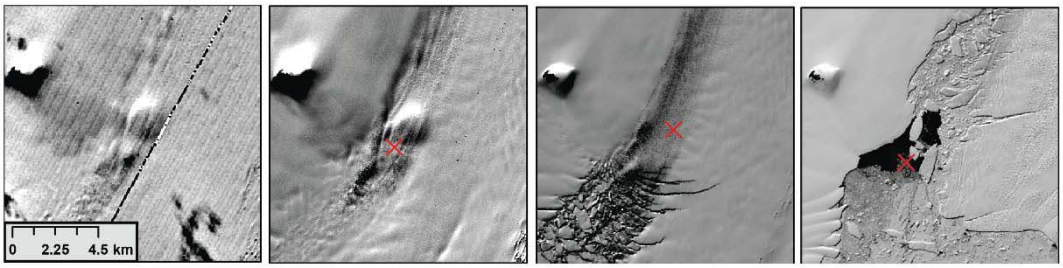

Pine Island- ID N/A

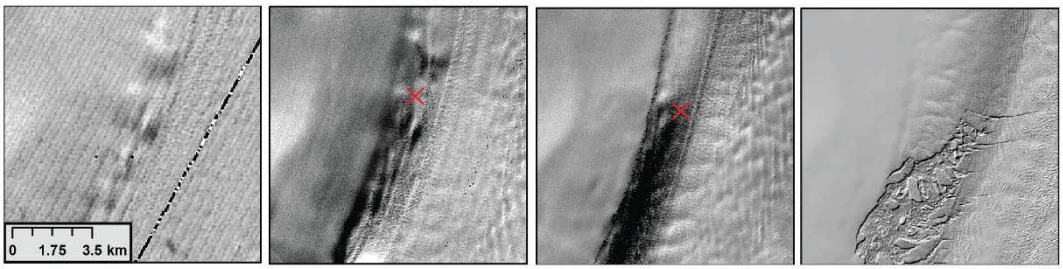

Pine Island- ID N/A

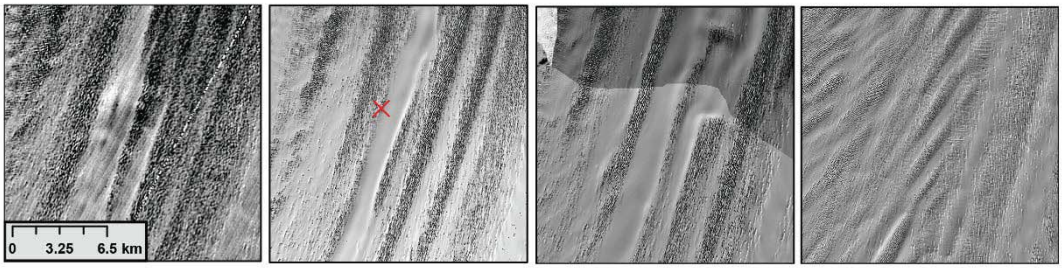

Pine Island- ID N/A

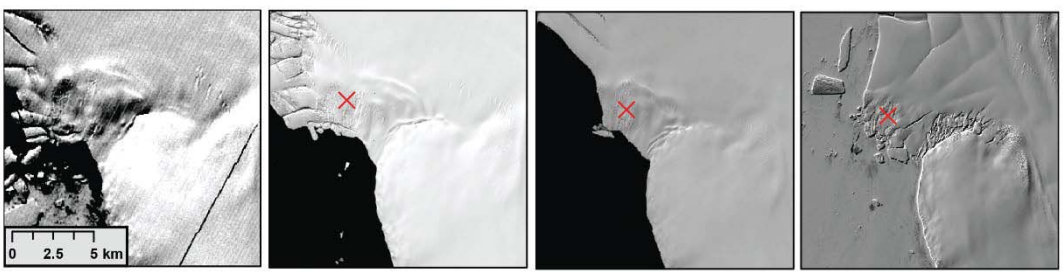

Pine Island- ID N/A

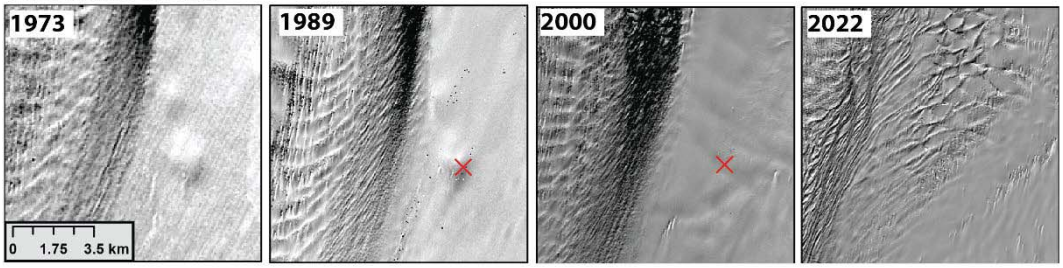

Crosson- Davis Ice Rise - ID 373-374

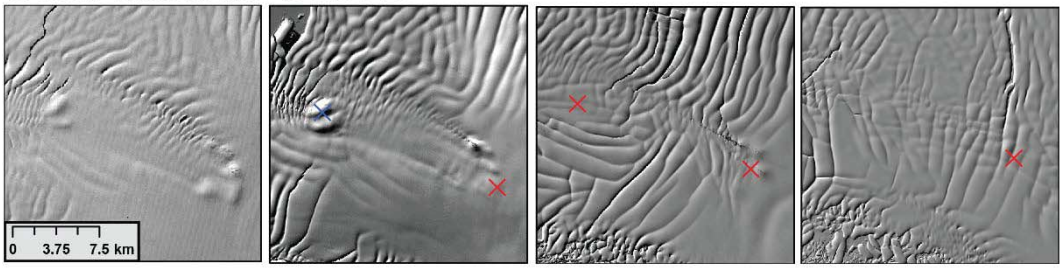

Dotson- ID 368

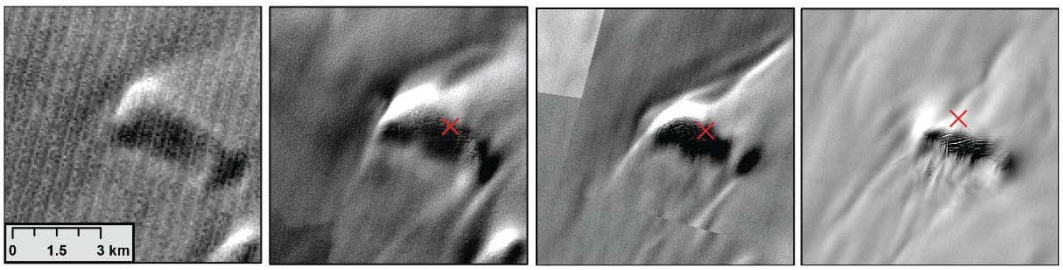

Dotson- ID N/A

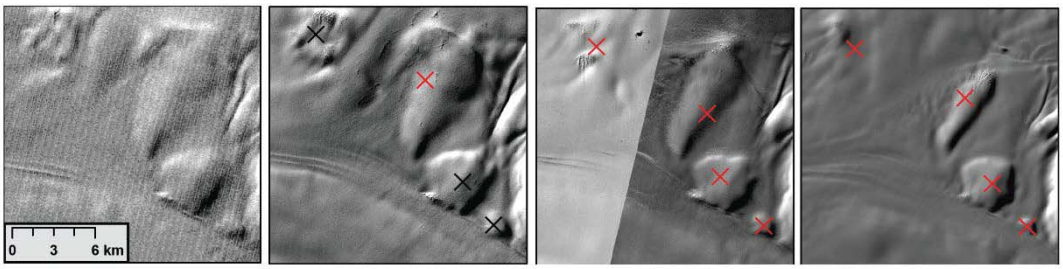

Dotson- Wunneburger Rock - ID 366

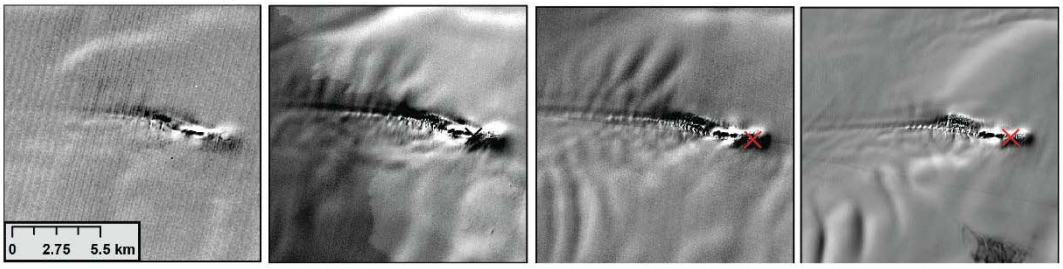

Pine Island- ID N/A

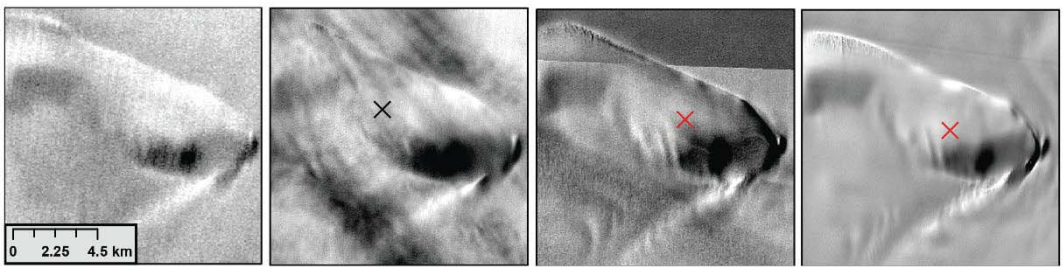

Getz- Nunn Island - ID 362

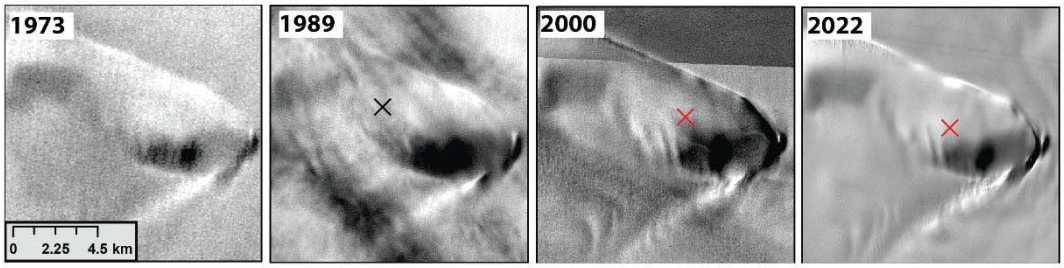

Getz- ID 359

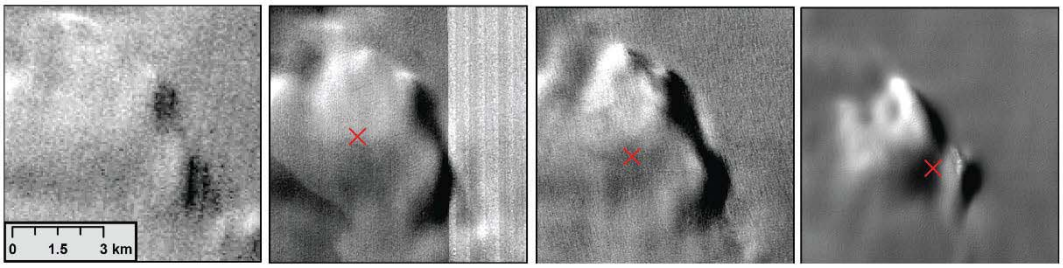

Getz- ID 353

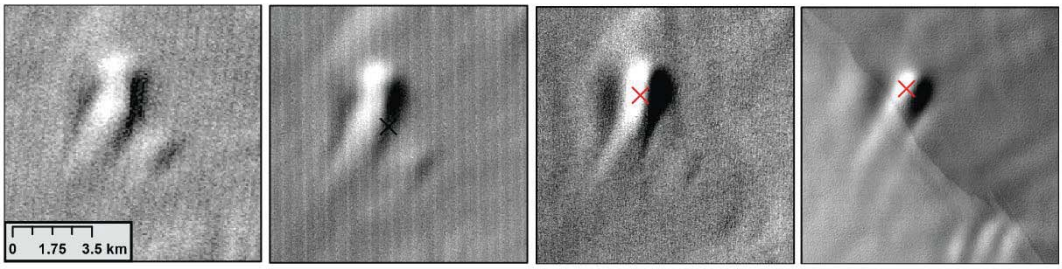

Getz- ID 348

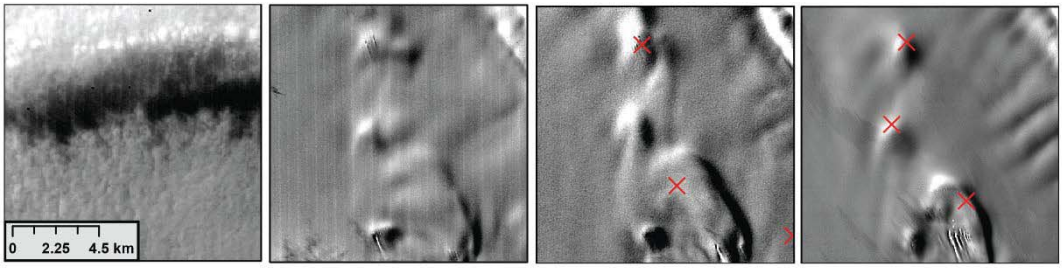

Getz- Dean Island - ID 347

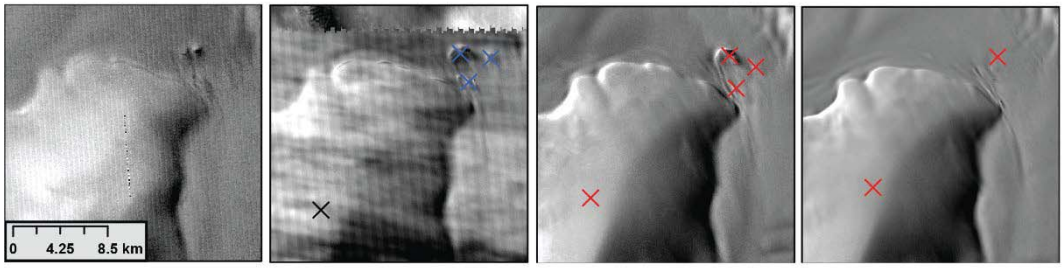

Getz- ID 346

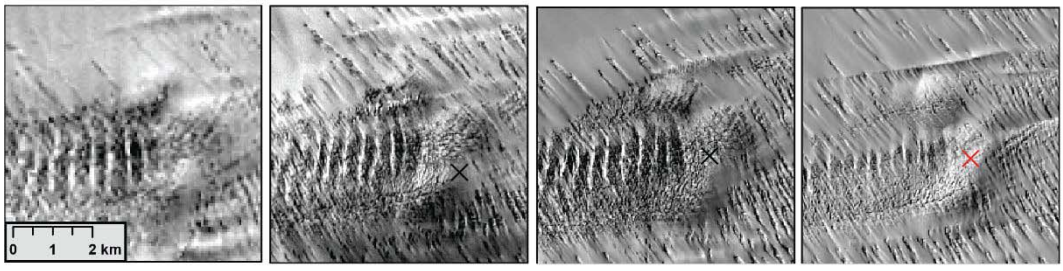

Getz- ID 339

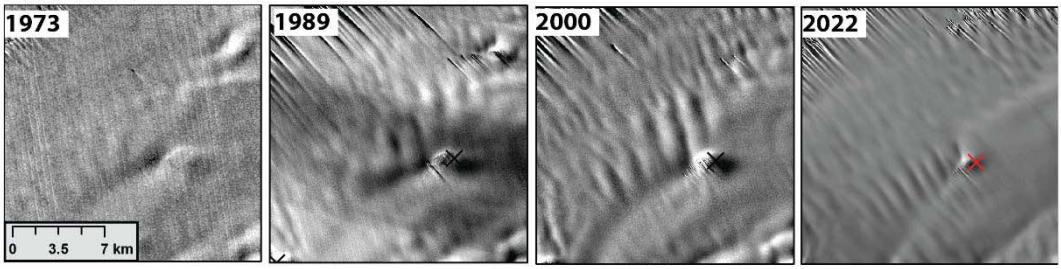

Getz- ID 340

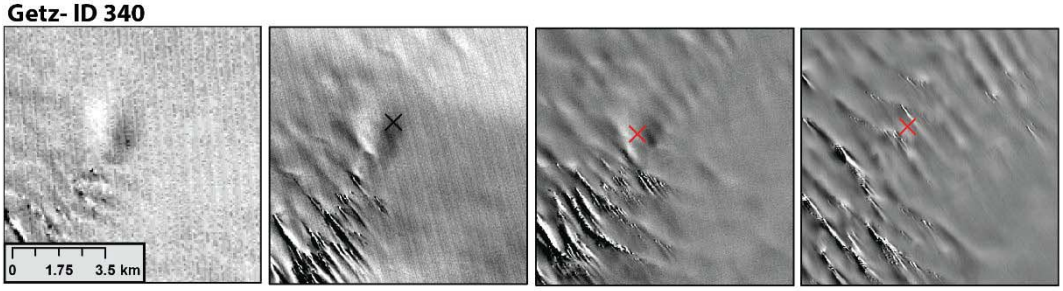

Hull- ID N/A

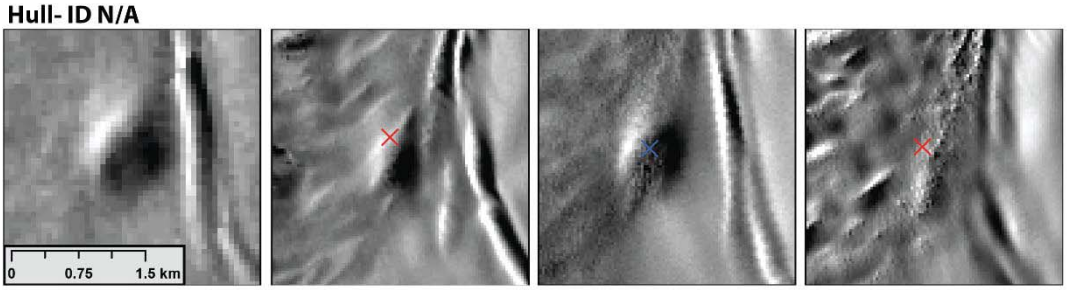

Hull- ID N/A

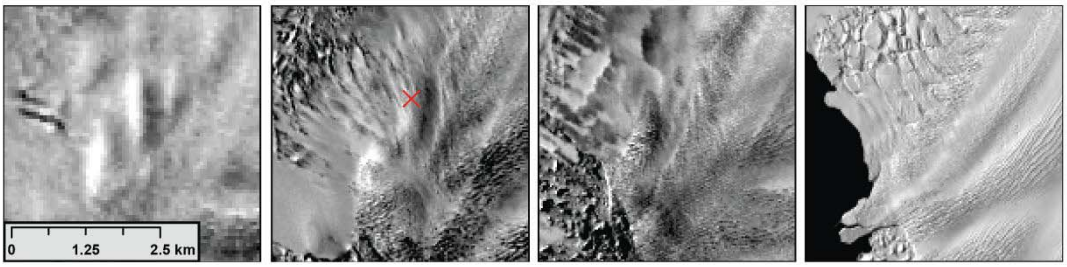

Nickerson- ID 330

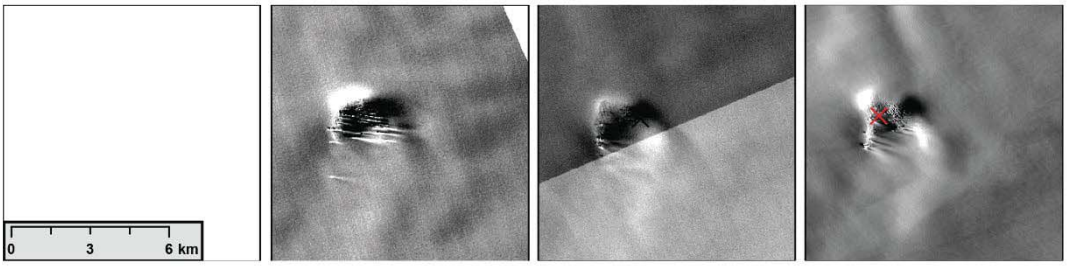

Sulzberger/Hammond Glacier - ID 327

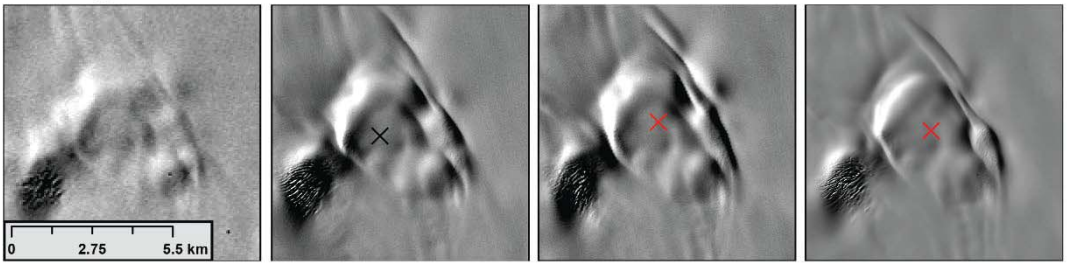

Sulzberger/Hammond Glacier- ID 325

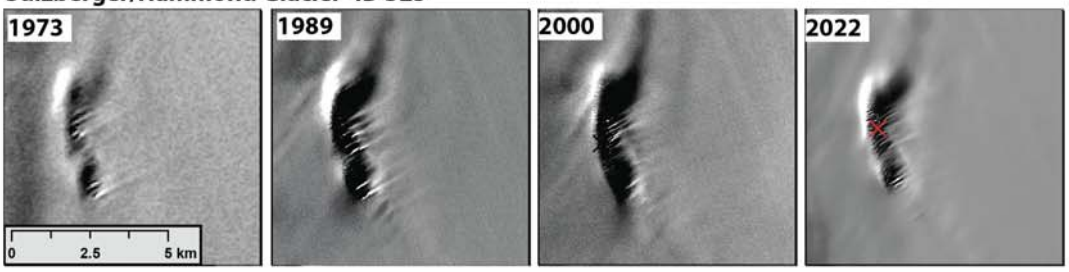

Sulzberger- ID 322

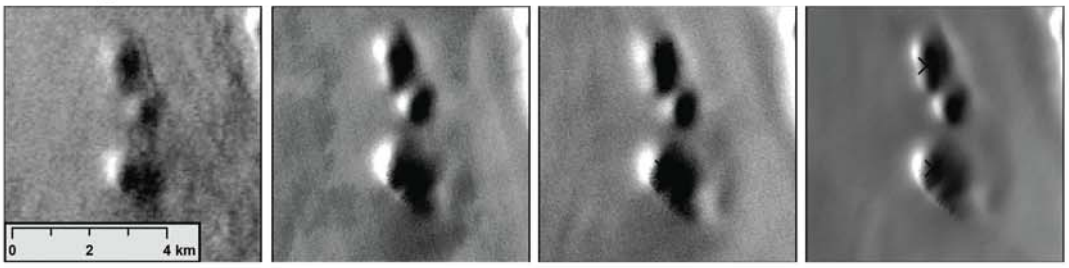

Sulzberger - Thode Island - ID 310

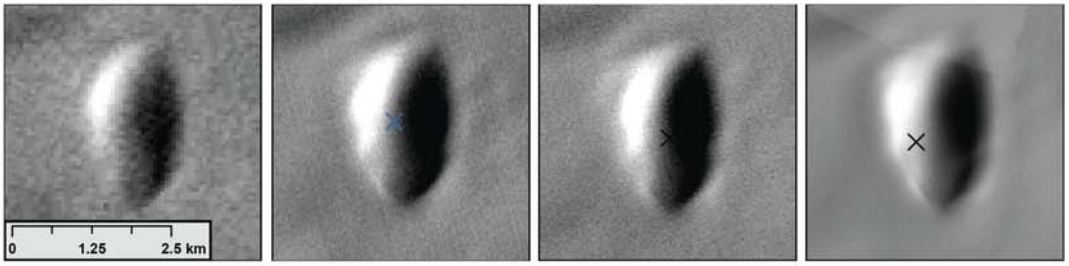

Sulzberger- ID 302

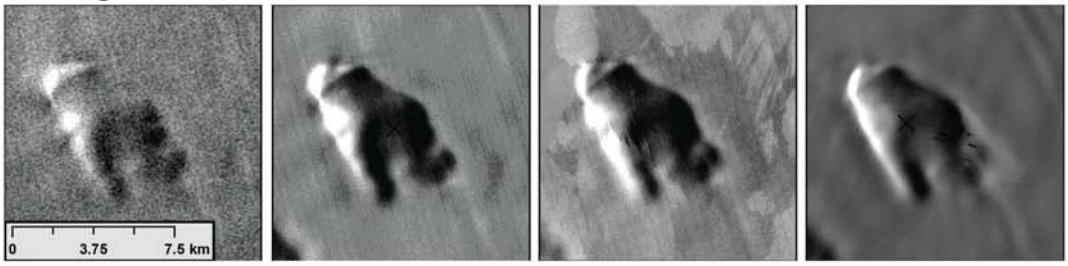

Sulzberger/Jacobel Glacier- ID 301

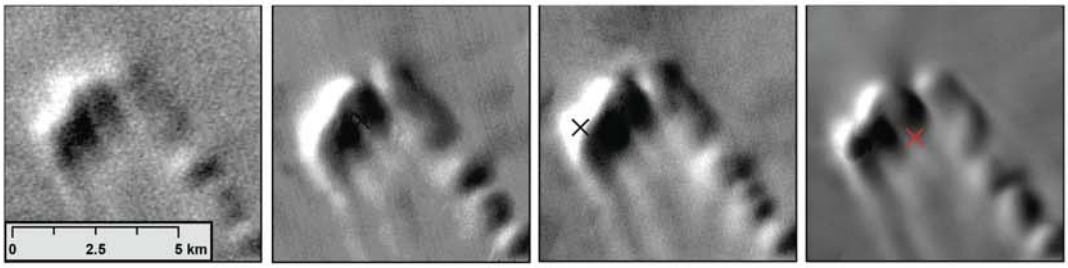

Swinburne/Buttler Glacier- ID 285

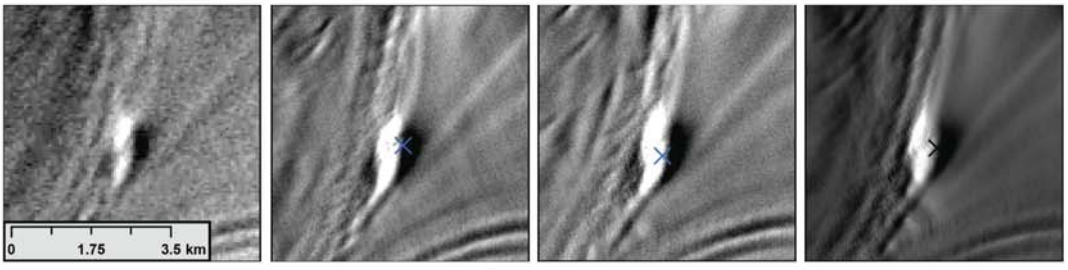

Richter- ID N/A

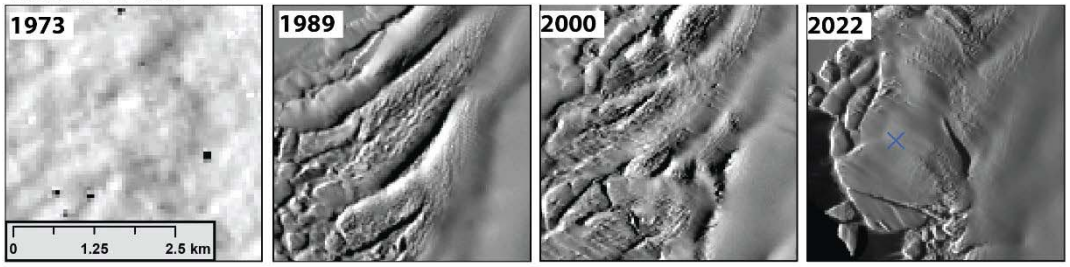

Ross- ID 253-254

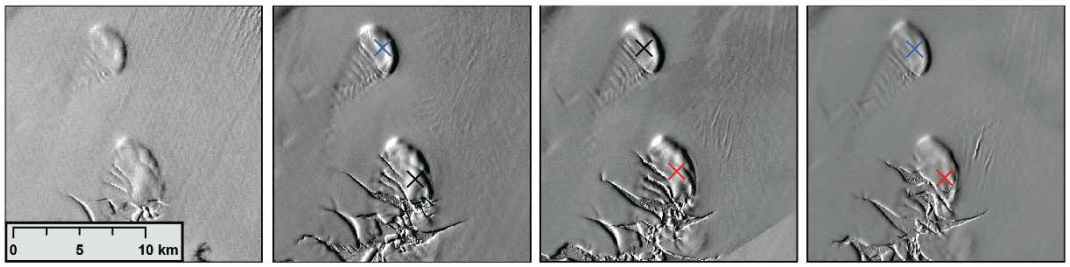

Ross- ID 255

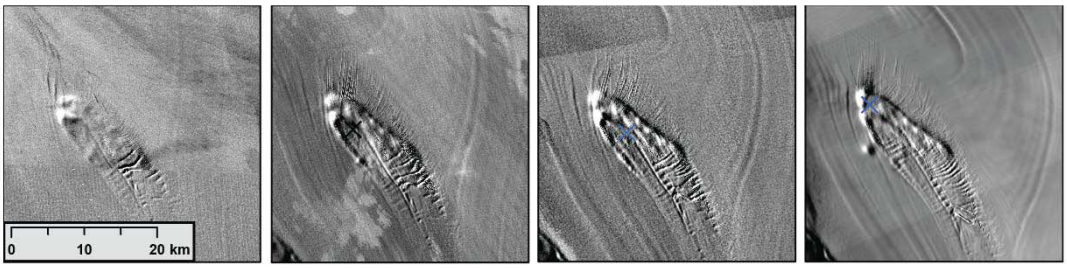

Ross/Kamb Ice Stream - Steershead Ice Rise - ID 257

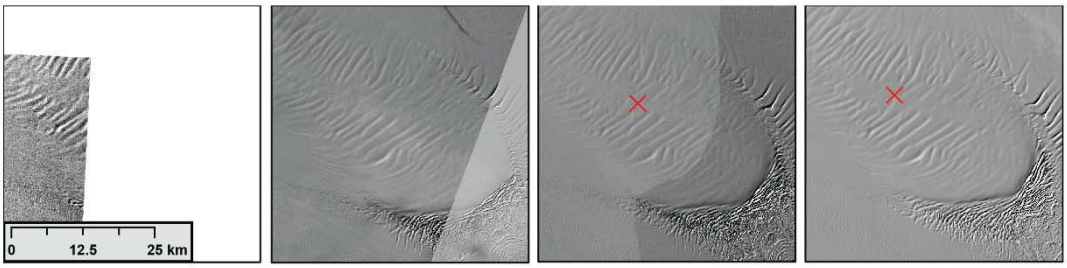

Ross- ID 259

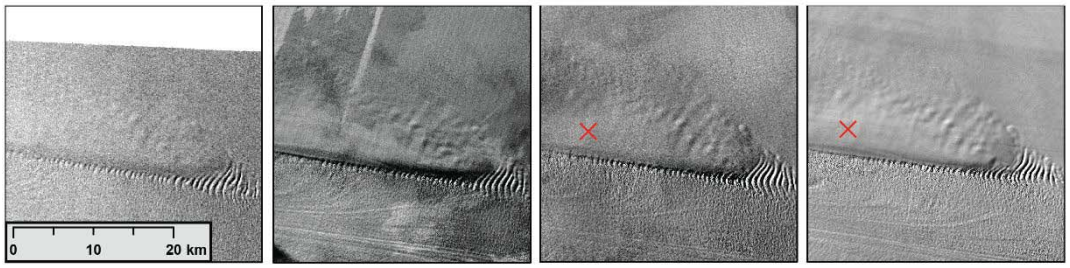

Ross/Kamb Ice Stream- ID 260

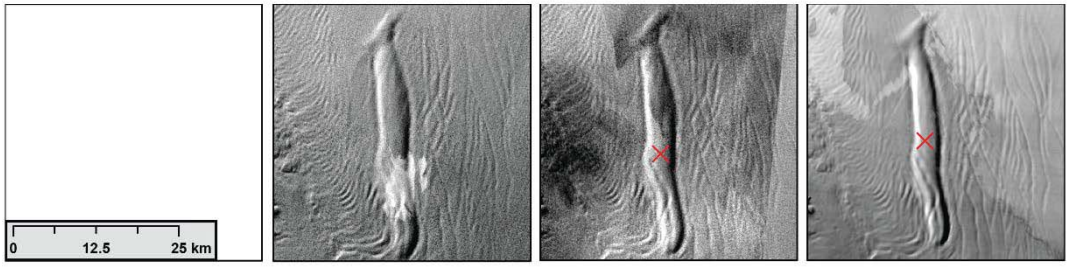

Ross- ID N/A

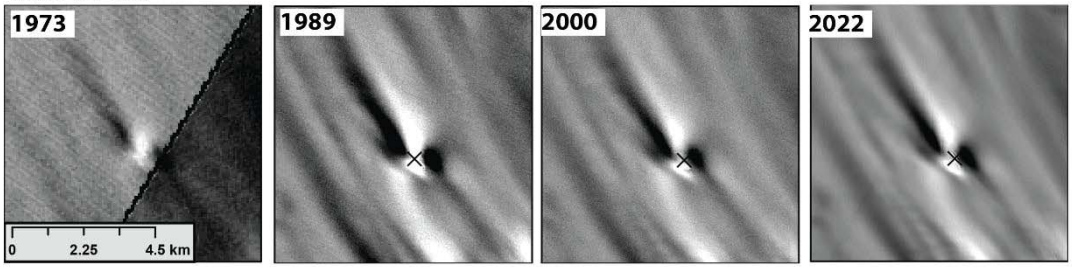

Ross- ID N/A

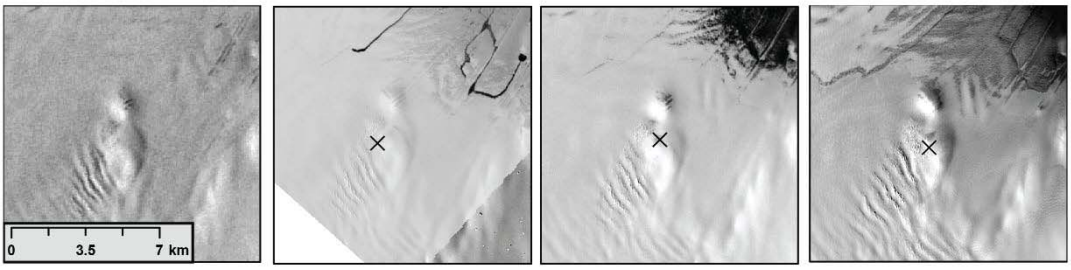

Campbell- ID 238

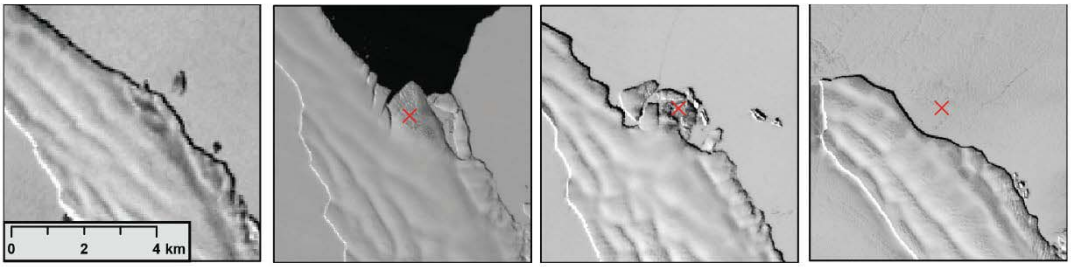

Rennick- ID 226

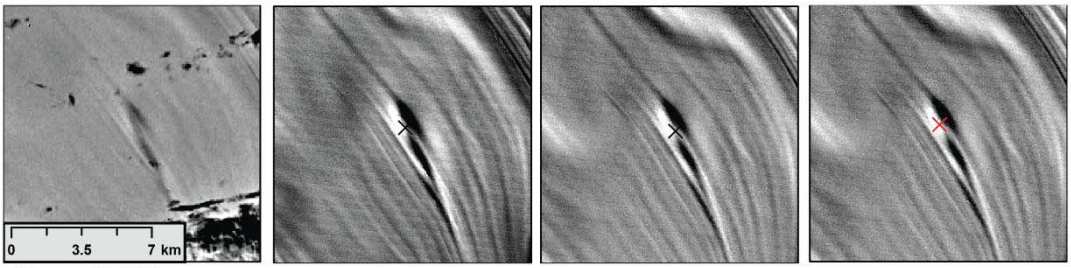

Slava- ID 220

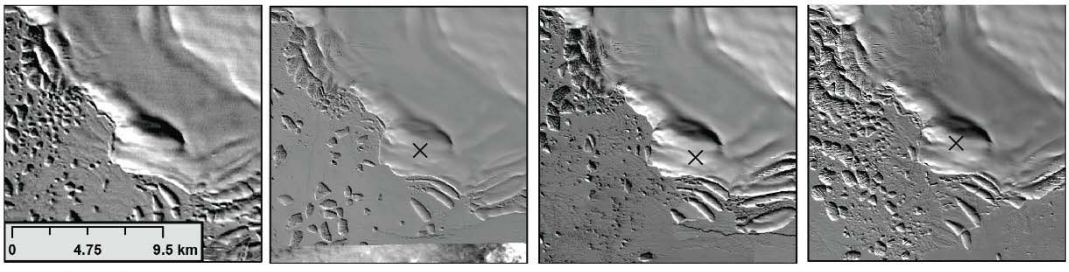

Cook- ID N/A

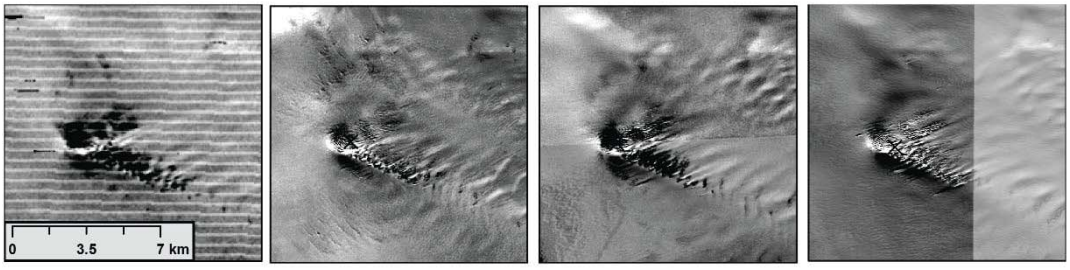

Holmes- ID 202

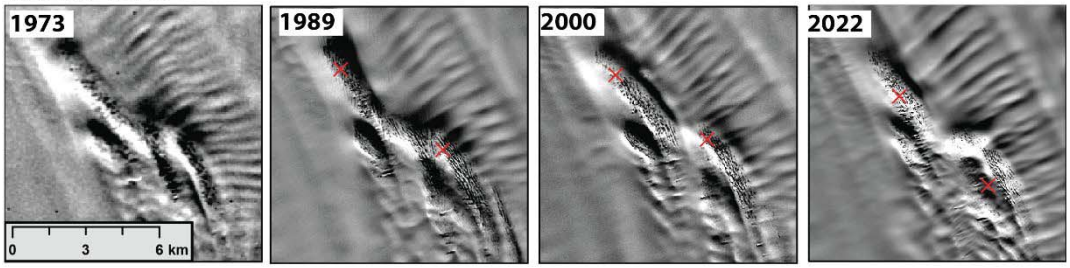

Holmes- ID N/A

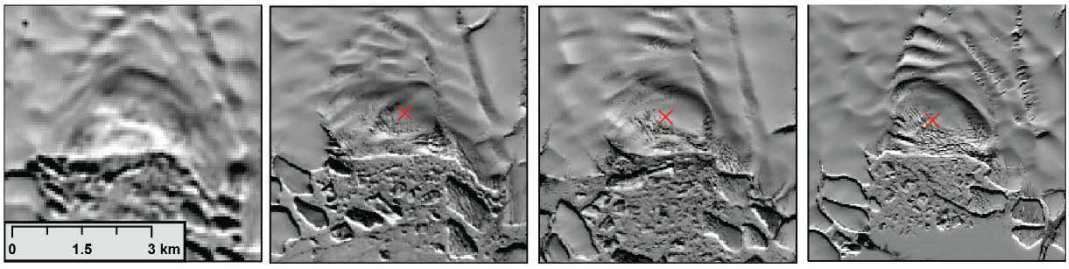

Moscow University - Henry Islands - ID 189,193

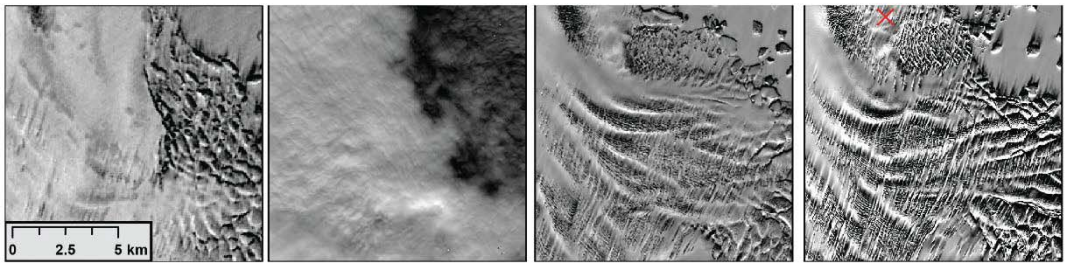

Moscow University - Henry Islands - ID 189,193

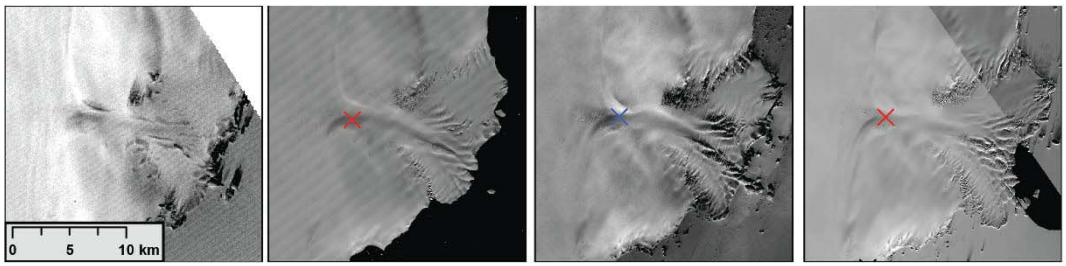

Totten- ID 180

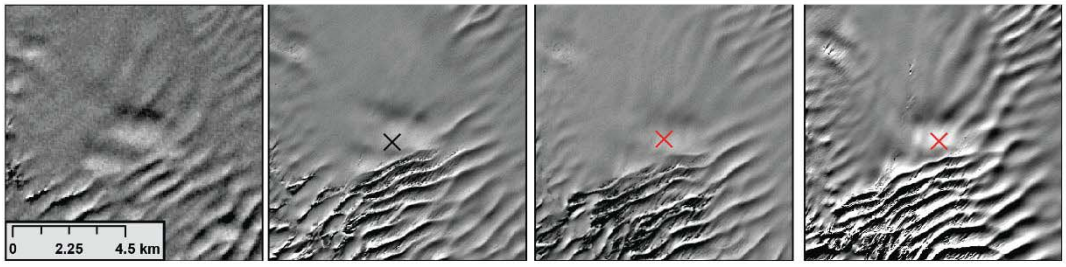

Totten- ID N/A

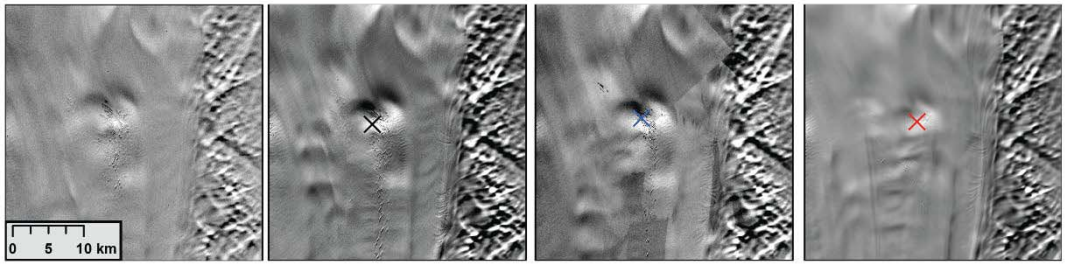

Totten- ID 183

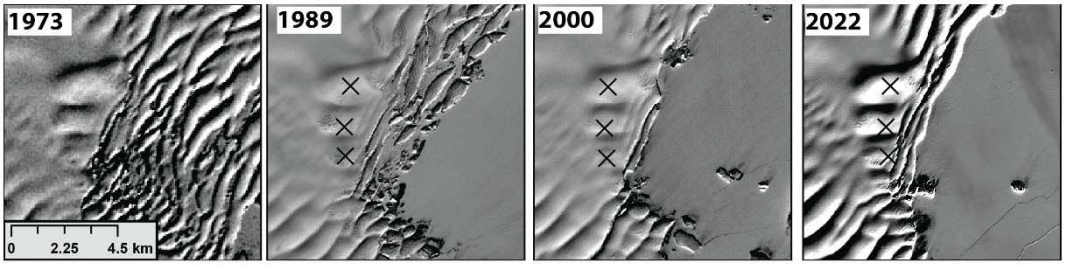

Conger - Bowman Island - ID 172-173

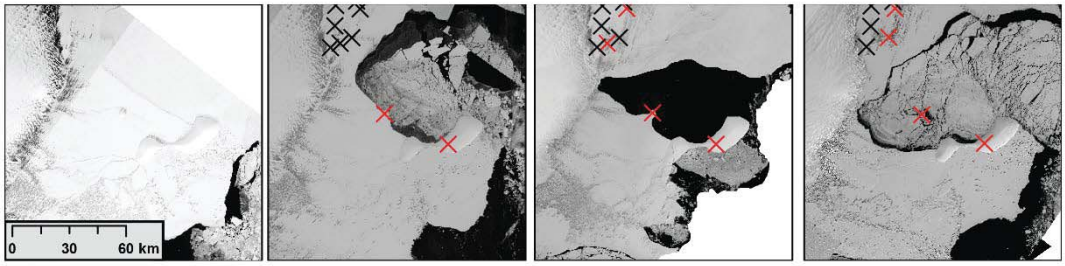

Shackleton- ID 161

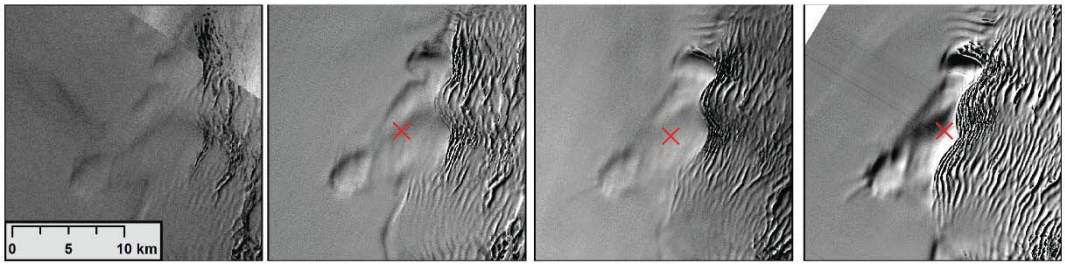

Shackleton/Denman Glacier - Chugunov Island - ID 167

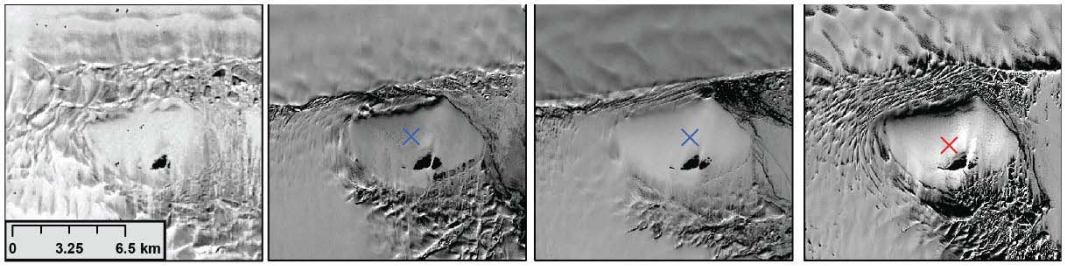

West- ID 149

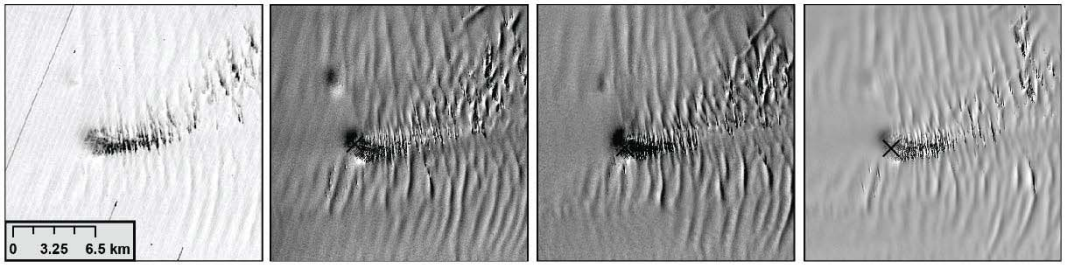

West- ID 146

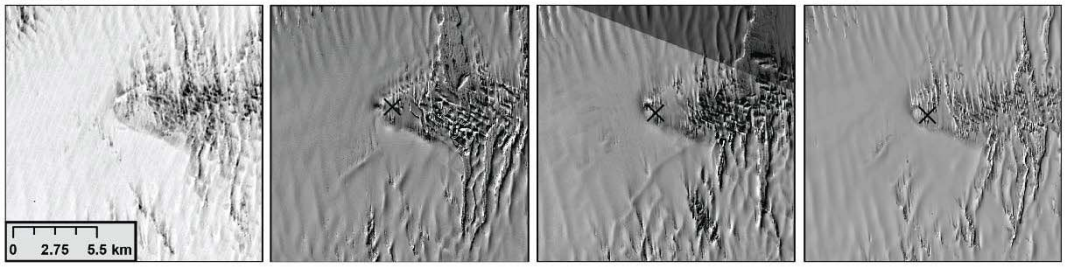

Amery- ID 111

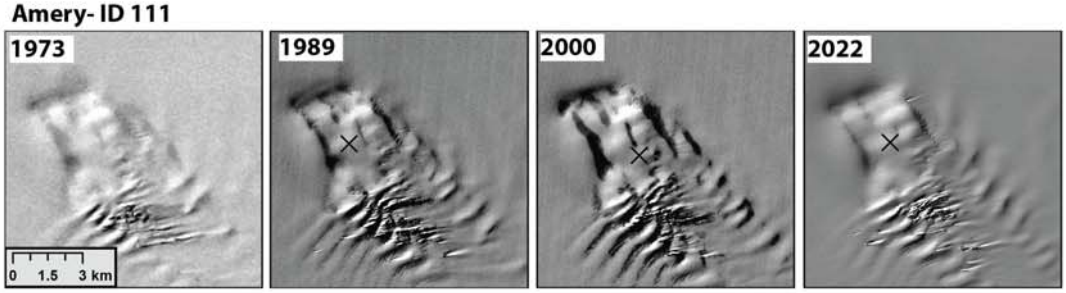

Amery - Tingy Rocks - ID 102

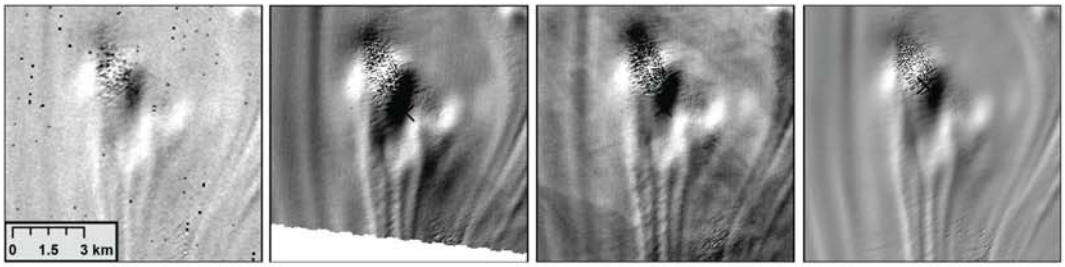

Amery- ID 109

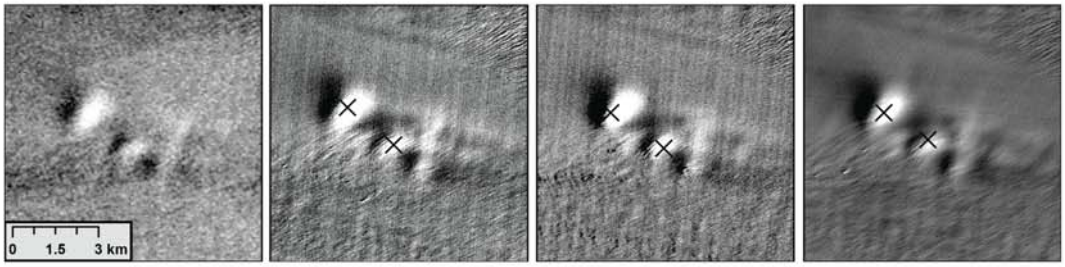

Wima-Robert-Downer- ID 93

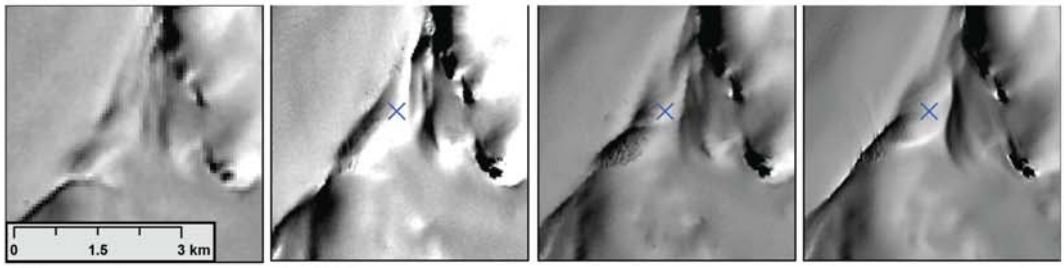

Wima-Robert-Downer- ID N/A

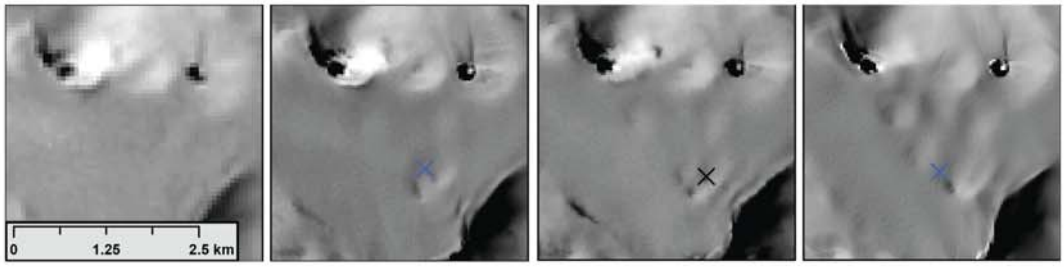

Wima-Robert-Downer- ID 90

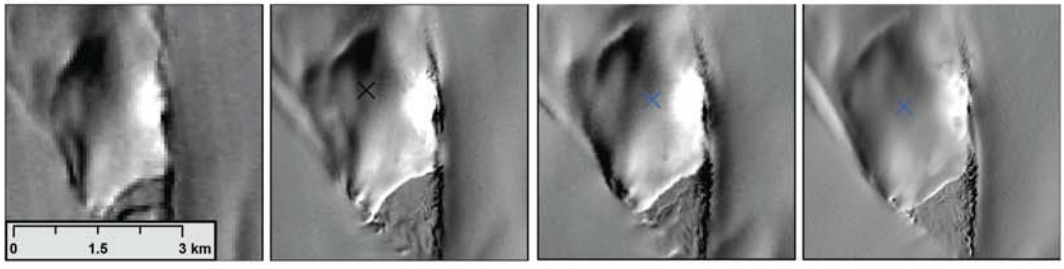

Wima-Robert-Downer- ID 92

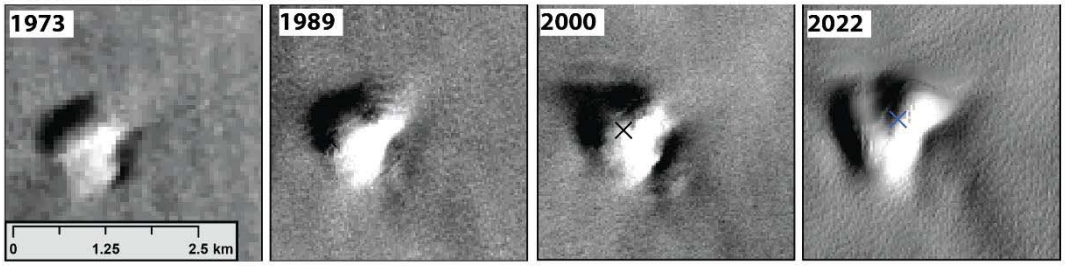

Prince Harald- ID 71

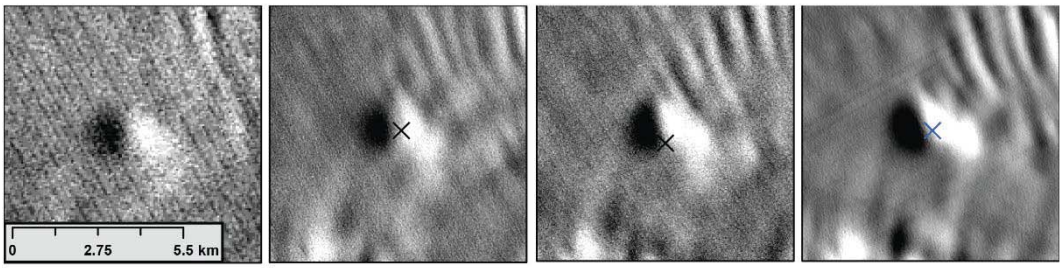

Prince Harald- ID 77

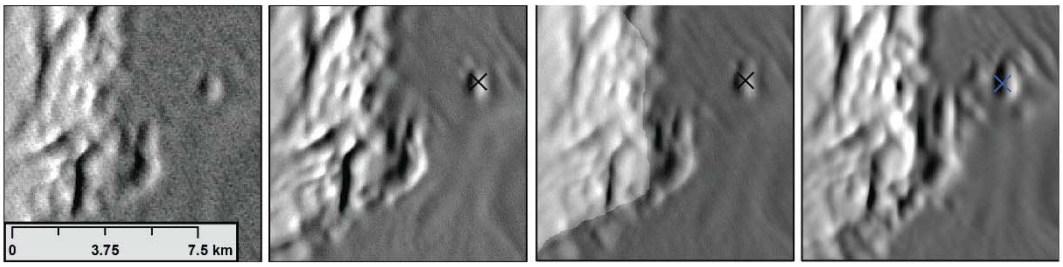

Roi Baudouin- ID 57

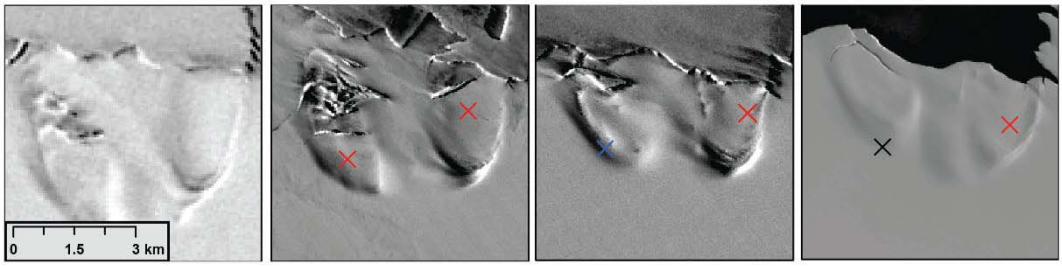

Roi Baudouin- ID 65-66

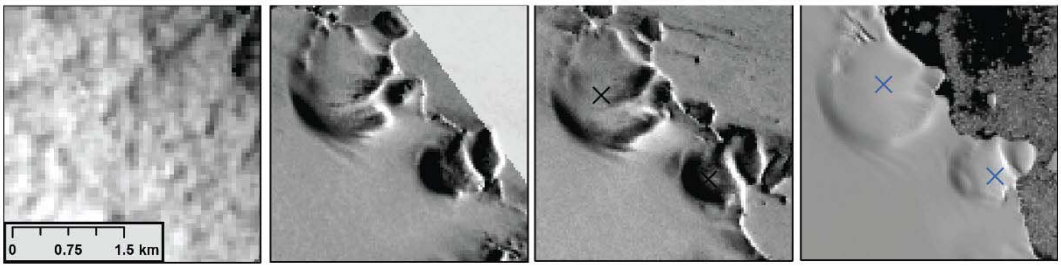

Lazarev - Kupol Verbljud Ice Rise - ID 33

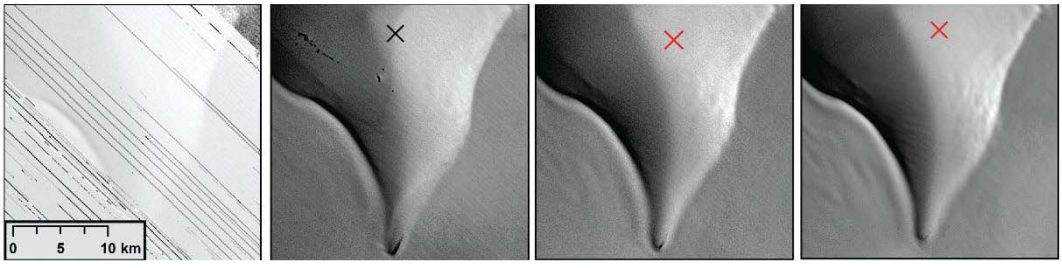

Lazarev- ID 31-32

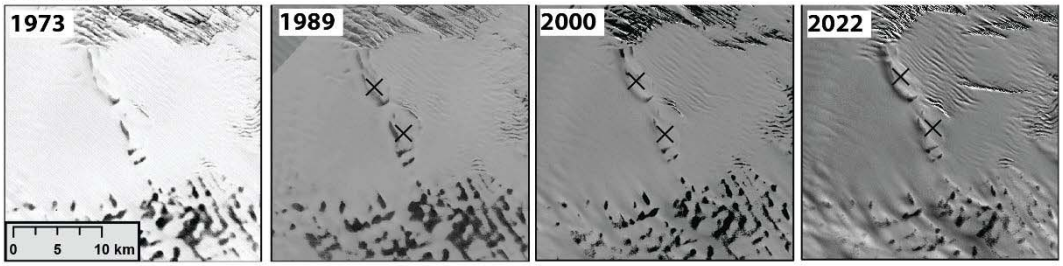

Nivilsen - Kuvklaken Ice Rise - ID 22

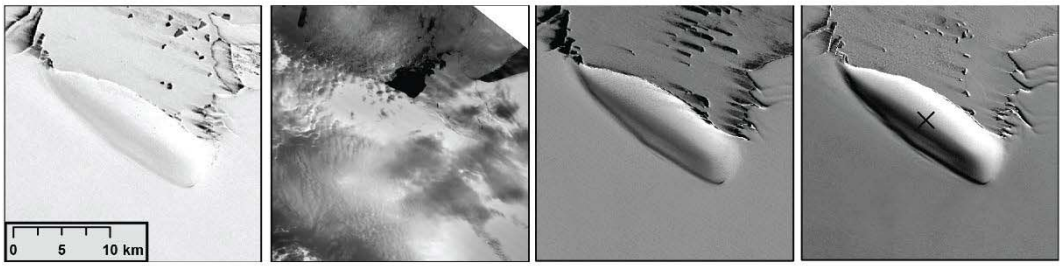

Nivilsen - Kupol Mira Ice Rise - ID 21

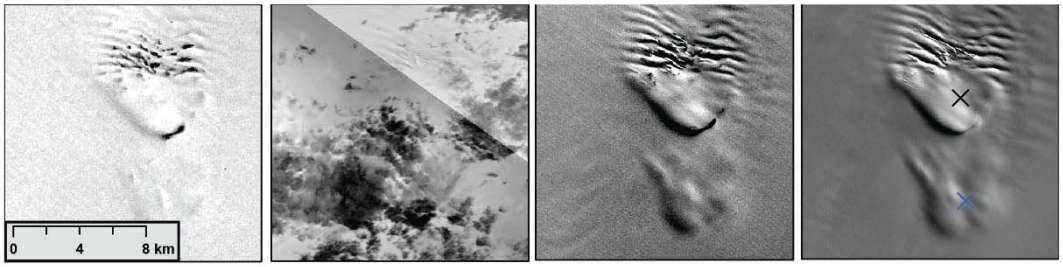

Fimbul - Kupol Khroska Ice Rise - ID 3

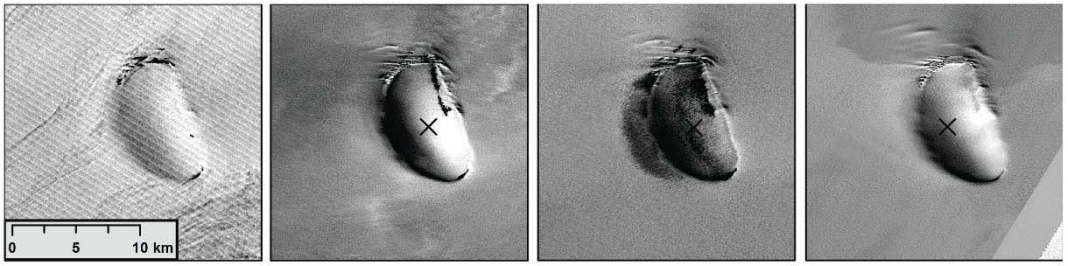

Fimbul- ID 701

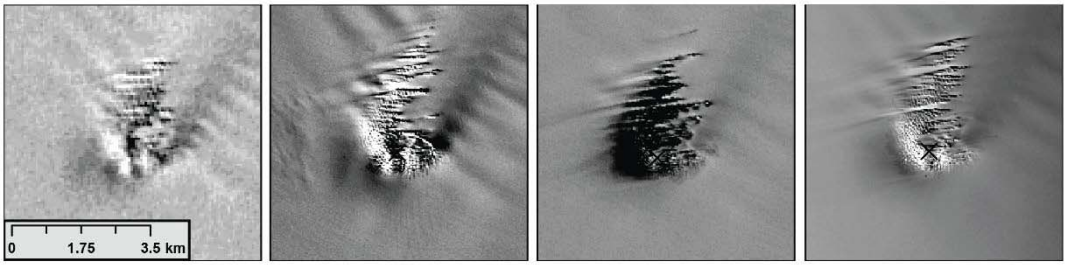

Jelbartisen - ID 693

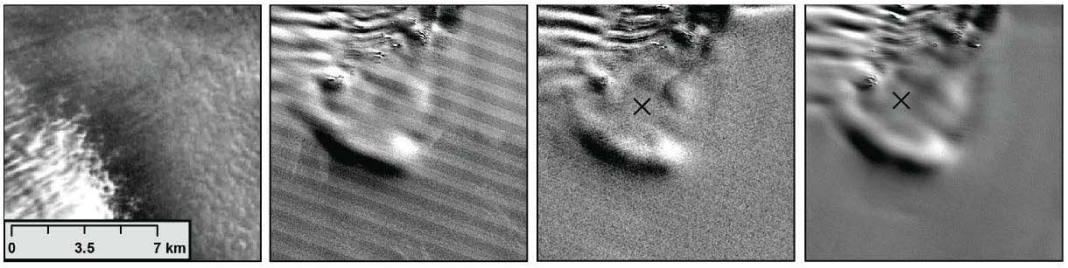

Ekström - Atkakuppelen Ice Rise - ID 688

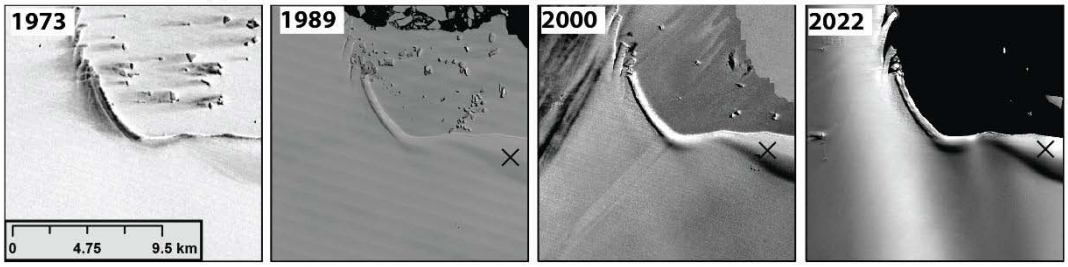

Riiser-Larsen- ID 674

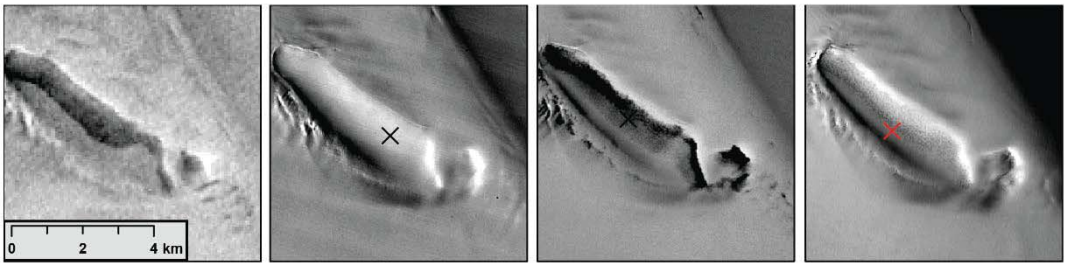

Riiser-Larsen- ID 666-669

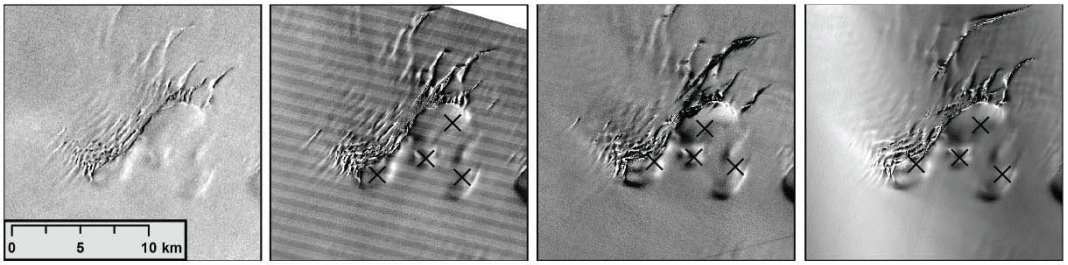

Riiser-Larsen- ID 662

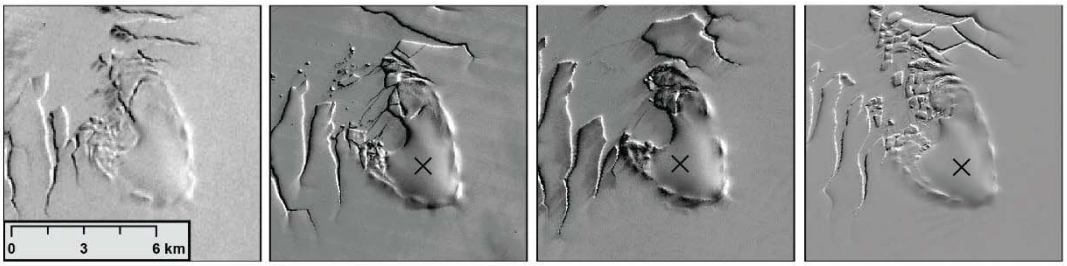

Riiser-Larsen- ID 663

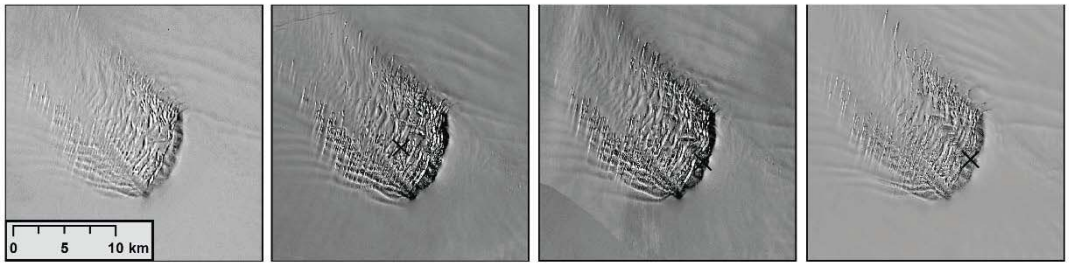

Brunt - McDonald Ice Rumples - ID 654

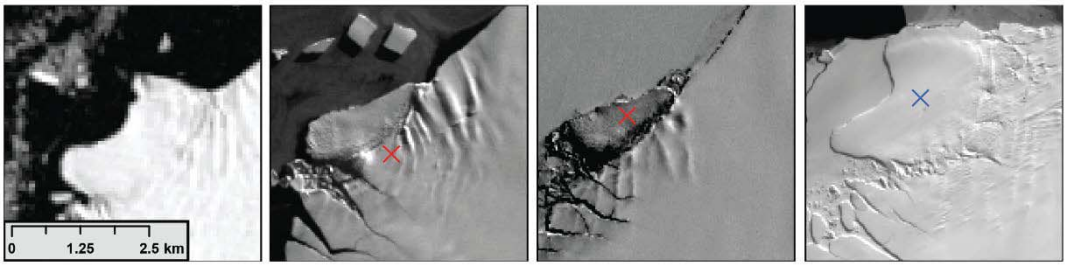

Filchner–Ronne- ID 644-655

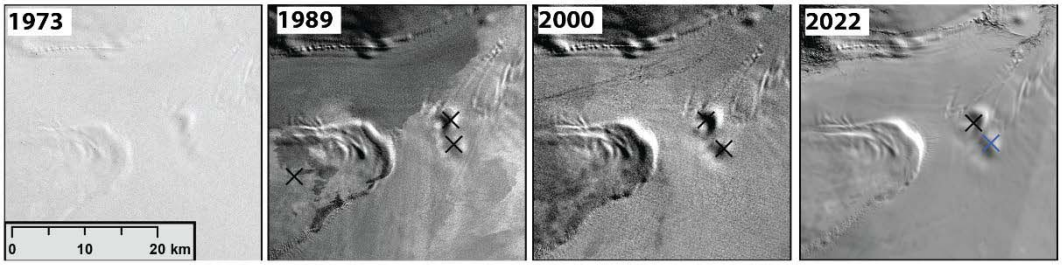

Filchner–Ronne- ID 641

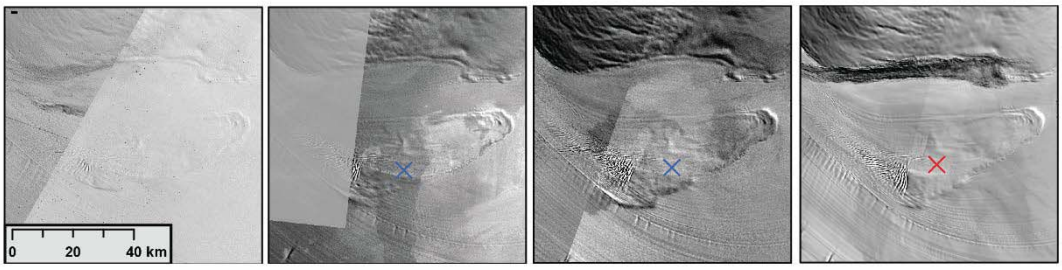

Filchner–Ronne- ID 642

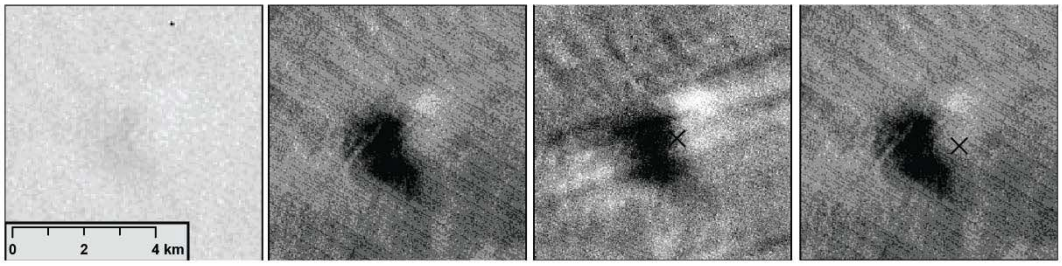

Filchner–Ronne - Doake Ice Rumples - ID 576 & 585

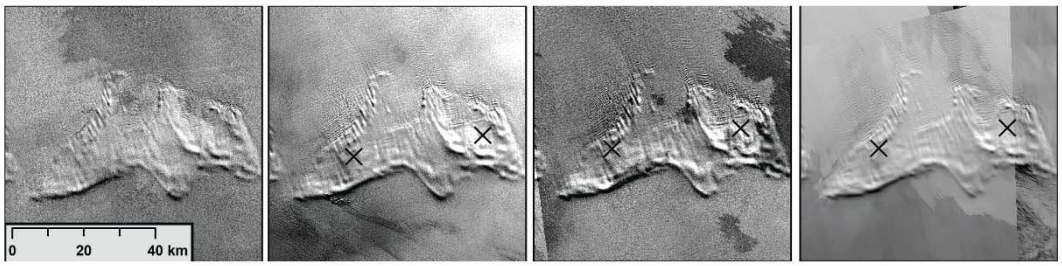

Filchner–Ronne- ID 471 & 474

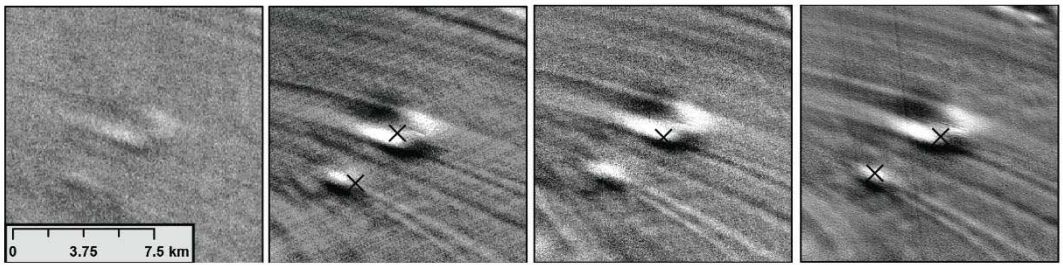

Filchner–Ronne - Kershaw Ice Rumples - ID 470

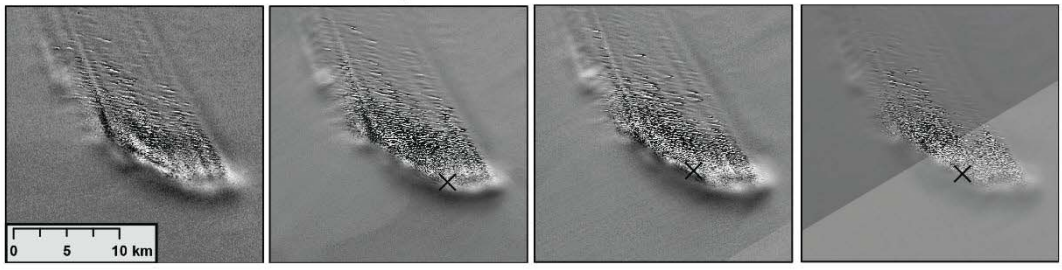

Landsat ID's used in 1973 mosaic	
LM01_L1GS_175119_19731105	LM01_L1GS_127107_19731115
LM01_L1GS_181118_19731116	LM01_L1GS_129107_19730115
LM01_L1GS_181119_19731116	LM01_L1GS_129108_19730115
LM01_L1GS_189119_19731211	LM01_L1GS_131107_19730204
LM01_L1GS_190117_19731211	LM01_L1GS_131108_19730204
LM01_L1GS_190118_19731211	LM01_L1GS_131109_19730204
LM01_L1GS_193119_19731110	LM01_L1GS_131110_19730204
LM01_L1GS_194117_19731110	LM01_L1GS_131111_19730204
LM01_L1GS_194118_19731110	LM01_L1GS_131112_19730204
LM01_L1GS_195116_19730127	LM01_L1GS_131113_19730204
LM01_L1GS_199119_19731110	LM01_L1GS_135111_19730316
LM01_L1GS_201116_19731117	LM01_L1GS_136111_19730227
LM01_L1GS_204116_19740113	LM01_L1GS_136112_19730227
LM01_L1GS_206116_19740202	LM01_L1GS_136113_19730227
LM01_L1GS_206118_19731210	LM01_L1GS_135112_19730316
LM01_L1GS_208118_19740204	LM01_L1GS_137109_19740223
LM01_L1GS_208119_19740204	LM01_L1GS_137110_19740223
LM01_L1GS_209117_19730211	LM01_L1GS_135109_19731211
LM01_L1GS_211115_19740207	LM01_L1GS_137111_19740223
LM01_L1GS_213115_19740209	LM01_L1GS_135110_19730316
LM01_L1GS_213118_19731217	LM01_L1GS_099107_19731104
LM01_L1GS_213119_19731217	LM01_L1GS_100107_19721215
LM01_L1GS_215116_19730217	LM01_L1GS_101107_19740117
LM01_L1GS_215117_19730217	LM01_L1GS_102107_19721219
LM01_L1GS_217116_19740213	LM01_L1GS_102108_19721219
LM01_L1GS_219114_19730220	LM01_L1GS_107107_19731026
LM01_L1GS_219115_19730220	LM01_L1GS_107108_19731026
LM01_L1GS_219116_19730220	LM01_L1GS_109106_19730131
LM01_L1GS_224115_19731210	LM01_L1GS_109107_19730131
LM01_L1GS_225114_19731210	LM01_L1GS_109108_19730131
LM01_L1GS_076109_19730220	LM01_L1GS_111107_19731117
LM01_L1GS_078109_19731101	LM01_L1GS_111108_19731117
LM01_L1GS_081109_19731104	LM01_L1GS_114107_19731015
LM01_L1GS_084108_19740118	LM01_L1GS_116106_19731104
LM01_L1GS_086108_19740207	LM01_L1GS_116107_19731104
LM01_L1GS_085107_19731214	LM01_L1GS_118106_19721129
LM01_L1GS_085108_19731214	LM01_L1GS_118107_19721129
LM01_L1GS_088107_19730304	LM01_L1GS_119107_19740223
LM01_L1GS_089107_19730128	LM01_L1GS_121107_19721202
LM01_L1GS_090107_19730129	LM01_L1GS_122106_19721202
LM01_L1GS_092107_19730218	LM01_L1GS_123106_19740227
LM01_L1GS_094107_19731030	LM01_L1GS_123107_19740227
LM01_L1GS_095107_19731013	LM01_L1GS_137108_19731231
LM01_L1GS_096107_19731101	LM01_L1GS_140108_19721221
LM01_L1GS_098106_19730101	LM01_L1GS_144107_19721207

LM01_L1GS_098107_19731103	LM01_L1GS_144108_19721207
LM01_L1GS_098107_19730101	LM01_L1GS_146108_19730219
LM01_L1GS_124107_19730215	LM01_L1GS_147107_19730202
LM01_L1GS_126107_19731114	LM01_L1GS_147108_19730202
LM01_L1GS_126108_19731114	LM01_L1GS_150107_19740218
LM01_L1GS_150108_19740218	LM01_L1GS_247112_19730107
LM01_L1GS_153108_19740116	LM02_L1GS_236112_19750218
LM01_L1GS_154107_19740117	LM03_L1GS_233110_19781229
LM01_L1GS_154108_19740117	LM01_L1GS_161110_19731113
LM01_L1GS_156108_19740101	LM01_L1GS_161111_19731113
LM01_L1GS_156109_19731214	LM01_L1GS_161112_19731113
LM01_L1GS_156110_19731214	LM01_L1GS_162110_19731114
LM01_L1GS_158109_19740121	LM01_L1GS_163109_19731115
LM01_L1GS_161109_19731113	LM01_L1GS_163110_19731115
LM01_L1GS_162109_19731114	LM01_L1GS_164110_19731116
LM01_L1GS_177110_19731111	LM01_L1GS_164111_19731116
LM01_L1GS_179110_19731113	LM01_L1GS_164112_19731116
LM01_L1GS_179111_19731113	LM01_L1GS_165109_19740128
LM01_L1GS_182110_19731204	LM01_L1GS_165110_19731117
LM01_L1GS_182111_19731204	LM01_L1GS_166109_19731118
LM01_L1GS_183111_19730310	LM01_L1GS_167110_19731119
LM01_L1GS_186110_19731102	LM01_L1GS_167111_19731119
LM01_L1GS_190113_19740222	LM01_L1GS_168110_19731120
LM01_L1GS_190114_19740222	LM01_L1GS_168111_19731120
LM01_L1GS_191111_19740118	LM01_L1GS_170110_19731210
LM01_L1GS_191112_19740118	LM02_L1GS_173109_19751019
LM01_L1GS_191113_19740118	LM02_L1GS_173110_19751124
LM01_L1GS_192114_19721218	LM02_L1GS_175110_19751126
LM01_L1GS_192115_19721218	LM02_L1GS_177109_19760208
LM01_L1GS_195112_19730127	LM01_L1GS_012119_19731107
LM01_L1GS_195114_19730127	LM01_L1GS_017119_19731107
LM01_L1GS_197113_19730110	LM01_L1GS_018114_19731219
LM01_L1GS_197113_19730216	LM01_L1GS_018118_19731219
LM02_L1GS_182111_19751028	LM01_L1GS_021114_19730114
LM02_L1GS_184110_19751030	LM01_L1GS_021115_19730114
LM02_L1GS_189110_19750225	LM01_L1GS_022115_19721228
LM02_L1GS_190110_19751123	LM01_L1GS_022116_19721228
LM01_L1GS_002111_19730113	LM01_L1GS_027113_19721214
LM01_L1GS_228112_19740206	LM01_L1GS_027116_19721214
LM01_L1GS_231112_19730109	LM01_L1GS_030116_19721129
LM01_L1GS_232110_19730109	LM01_L1GS_030117_19731126
LM01_L1GS_232111_19730109	LM01_L1GS_032117_19731127
LM01_L1GS_232113_19730109	LM01_L1GS_033115_19721203
LM01_L1GS_233109_19740106	LM02_L1GS_018119_19751130
LM01_L1GS_233111_19730129	LM02_L1GS_023114_19751205
LM01_L1GS_233112_19730129	LM02_L1GS_025115_19760217

LM01_L1GS_233113_19730129	LM02_L1GS_025116_19760217
LM01_L1GS_235113_19730112	LM01_L1GS_046118_19740116
LM01_L1GS_236109_19740109	LM02_L1GS_051116_19751109
LM01_L1GS_237110_19721121	LM01_L1GS_046119_19740116
LM01_L1GS_237111_19721121	LM01_L1GS_050118_19731127
LM01_L1GS_237113_19730115	LM01_L1GS_051116_19721221
LM01_L1GS_240112_19740131	LM01_L1GS_051116_19740103
LM01_L1GS_243112_19730121	LM01_L1GS_051117_19740103
LM01_L1GS_247111_19730107	LM01_L1GS_052116_19740104
LM01_L1GS_052117_19740104	LM02_L1GS_249113_19750213
LM01_L1GS_053116_19740105	LM01_L1GS_006113_19721230
LM01_L1GS_053117_19740105	LM01_L1GS_010113_19731123
LM01_L1GS_054116_19721224	LM01_L1GS_010114_19731123
LM01_L1GS_055117_19730130	LM01_L1GS_014114_19731127
LM01_L1GS_055117_19740107	LM01_L1GS_018113_19730111
LM01_L1GS_056116_19730113	LM01_L1GS_019113_19730111
LM01_L1GS_056116_19740108	LM01_L1GS_019114_19730111
LM01_L1GS_056117_19740126	LM01_L1GS_020113_19721120
LM01_L1GS_057116_19730113	LM01_L1GS_020114_19721120
LM01_L1GS_058116_19731223	LM01_L1GS_022113_19730114
LM01_L1GS_064114_19730102	LM01_L1GS_246114_19730124
LM01_L1GS_064114_19740116	LM01_L1GS_248114_19730213
LM01_L1GS_065111_19721128	LM01_L1GS_004114_19730116
LM01_L1GS_065112_19721128	
LM01_L1GS_065113_19721128	
LM01_L1GS_065114_19721128	
LM01_L1GS_066114_19740117	
LM01_L1GS_067110_19721201	
LM01_L1GS_067111_19721201	
LM01_L1GS_067112_19721201	
LM01_L1GS_068110_19730125	
LM01_L1GS_068111_19721202	
LM01_L1GS_070111_19730108	
LM01_L1GS_071110_19721205	
LM01_L1GS_072110_19731026	
LM01_L1GS_073110_19740124	
LM02_L1GS_042117_19751206	
LM02_L1GS_050116_19751021	
LM01_L1GS_001112_19721207	
LM01_L1GS_001112_19730130	
LM01_L1GS_001113_19730130	
LM01_L1GS_001114_19730130	
LM01_L1GS_002113_19730113	
LM01_L1GS_003112_19721227	
LM01_L1GS_003113_19721227	
LM01_L1GS_003114_19730113	

Landsat ID's used in 1973 mosaic	
LT04_L1GS_038116_19880221	LT05_L1GS_082108_19890102
LT05_L1GS_156110_19861203	LT04_L1GS_088106_19890205
LT04_L1GS_155108_19891110	LT04_L1GS_088107_19890205
LT04_L1GS_155109_19891110	LT04_L1GS_087107_19890318
LT04_L1GS_157109_19890124	LT04_L1GS_084107_19900127
LT04_L1GS_157110_19891108	LT04_L1GS_084108_19900127
LT04_L1GS_157111_19891108	LT04_L1GS_092106_19891218
LT04_L1GS_155110_19891212	LT04_L1GS_092107_19891218
LT04_L1GS_159109_19900125	LT04_L1GS_090106_19900121
LT04_L1GS_163109_19891204	LT04_L1GS_090107_19900121
LT04_L1GS_163110_19891204	LT05_L1GS_080108_19890104
LT04_L1GS_163111_19891204	LT05_L1GS_094107_19910213
LT04_L1GS_161109_19890325	LT04_L1GS_045116_19891225
LT04_L1GS_161110_19890325	LT04_L1GS_045117_19891225
LT04_L1GS_165109_19880215	LT04_L1GS_045118_19891225
LT04_L1GS_153109_19891128	LT04_L1GS_045119_19891225
LT04_L1GS_159110_19900125	LT04_L1GS_050116_19890227
LT04_L1GS_167109_19880128	LT04_L1GS_055115_19881212
LT04_L1GS_167110_19880128	LT04_L1GS_035119_19900120
LT04_L1GS_217103_19890128	LT04_L1GS_035120_19900120
LT04_L1GS_221108_19891124	LT04_L1GS_050115_19900129
LT04_L1GS_215103_19890319	LT04_L1GS_050117_19900129
LT05_L1GS_217106_19860301	LT04_L1GS_050118_19900129
LT04_L1GS_219105_19891126	LT04_L1GS_050119_19900129
LT05_L1GS_217107_19860301	LT04_L1GS_055116_19890129
LT05_L1GS_217108_19860301	LT04_L1GS_055117_19890129
LT05_L1GS_217105_19860301	LT04_L1GS_060113_19881215
LT04_L1GS_217104_19890128	LT04_L1GS_060114_19881215
LT04_L1GS_219104_19901215	LT04_L1GS_060115_19881215
LT04_L1GS_215104_19880229	LT04_L1GS_062112_19891114
LT04_L1GS_215105_19880229	LT04_L1GS_062113_19900117
LT04_L1GS_219106_19891126	LT04_L1GS_062114_19900117
LT04_L1GS_210111_19890127	LT04_L1GS_062115_19900117
LT04_L1GS_210112_19890127	LT04_L1GS_064110_19891128
LT04_L1GS_214108_19880206	LT04_L1GS_065111_19891119
LT04_L1GS_215107_19880112	LT04_L1GS_066109_19891228
LT04_L1GS_215109_19880128	LT04_L1GS_066110_19891228
LT04_L1GS_219108_19891212	LT04_L1GS_068110_19900111
LT04_L1GS_219109_19891212	LT04_L1GS_068111_19900111
LT05_L1GS_219107_19890219	LT04_L1GS_070109_19890207
LT04_L1GS_215108_19880128	LT04_L1GS_070110_19890207
LT04_L1GS_217109_19900115	LT05_L1GS_062111_19910128
LT04_L1GS_213110_19890321	LT04_L1GS_105107_19891112
LT05_L1GS_220107_19860218	LT04_L1GS_096106_19891231
LT05_L1GS_074109_19910217	LT04_L1GS_096107_19891231

LT04_L1GS_072109_19890221	LT04_L1GS_096108_19891231
LT04_L1GS_076108_19891116	LT04_L1GS_098107_19900130
LT04_L1GS_076109_19891116	LT04_L1GS_100107_19891227
LT04_L1GS_078108_19890303	LT04_L1GS_102107_19891107
LT05_L1GS_082107_19890102	LT04_L1GS_102108_19891107
LT04_L1GS_104107_19891121	LT04_L1GS_024113_19881219
LT04_L1GS_105106_19891112	LT04_L1GS_232113_19900124
LT04_L1GS_114105_19890228	LT04_L1GS_012113_19880114
LT04_L1GS_114106_19890228	LT04_L1GS_021113_19880214
LT04_L1GS_114107_19891111	LT04_L1GS_004113_19890209
LT04_L1GS_110106_19891115	LT04_L1GS_006113_19900109
LT04_L1GS_110107_19891115	LT04_L1GS_004114_19890209
LT04_L1GS_108107_19890218	LT04_L1GS_008112_19891222
LT04_L1GS_112106_19891113	LT04_L1GS_024112_19881219
LT04_L1GS_112107_19891113	LT04_L1GS_139107_19880124
LT05_L1GS_116106_19910208	LT04_L1GS_130108_19890316
LT04_L1GS_169109_19891214	LT04_L1GS_133108_19900220
LT04_L1GS_173109_19891108	LT04_L1GS_135107_19891114
LT04_L1GS_173110_19900228	LT04_L1GS_135108_19891114
LT04_L1GS_177109_19891120	LT04_L1GS_137107_19891112
LT05_L1GS_176109_19871015	LT04_L1GS_137108_19900131
LT04_L1GS_171109_19900214	LT04_L1GS_141106_19891124
LT05_L1GS_183113_19860130	LT04_L1GS_141107_19900212
LT04_L1GS_185114_19890317	LT04_L1GS_143106_19890327
LT04_L1GS_170110_19891221	LT04_L1GS_143107_19890327
LT04_L1GS_170111_19891221	LT04_L1GS_143108_19890327
LT04_L1GS_169110_19891214	LT04_L1GS_145107_19900312
LT04_L1GS_171110_19900113	LT04_L1GS_145108_19900312
LT04_L1GS_173111_19900228	LT04_L1GS_147108_19880217
LT04_L1GS_179110_19900121	LT04_L1GS_148108_19890125
LT04_L1GS_179111_19900206	LT04_L1GS_149109_19880215
LT04_L1GS_177110_19871030	LT04_L1GS_151108_19890215
LT04_L1GS_181111_19900119	LT04_L1GS_151109_19890215
LT04_L1GS_181112_19900119	LT04_L1GS_151110_19890215
LT04_L1GS_185113_19890317	LT04_L1GS_149108_19880114
LT04_L1GS_181114_19900220	LT04_L1GS_153108_19880110
LT04_L1GS_183111_19900117	LT04_L1GS_183116_19900101
LT04_L1GS_183113_19900117	LT04_L1GS_185116_19890301
LT04_L1GS_183115_19900101	LT04_L1GS_189117_19900127
LT04_L1GS_181113_19900119	LT04_L1GS_190115_19890216
LT05_L1GS_176110_19871015	LT04_L1GS_190117_19890131
LT04_L1GS_183112_19891114	LT04_L1GS_190118_19890131
LT04_L1GS_021112_19890115	LT04_L1GS_195115_19891204
LT04_L1GS_018112_19890211	LT04_L1GS_195116_19891204
LT04_L1GS_018113_19890211	LT04_L1GS_199114_19890130
LT04_L1GS_015113_19900124	LT04_L1GS_199115_19890130

LT04_L1GS_001112_19891221	LT04_L1GS_190116_19890131
LT04_L1GS_001113_19891221	LT04_L1GS_207113_19880308
LT04_L1GS_004112_19891226	LT04_L1GS_207114_19880308
LT04_L1GS_008113_19900123	LT04_L1GS_207115_19880308
LT04_L1GS_004113_19880122	LT04_L1GS_207116_19880308
LT04_L1GS_004114_19880122	LT04_L1GS_210116_19890127
LT04_L1GS_010112_19891220	LT04_L1GS_210117_19890127
LT04_L1GS_010113_19891220	LT04_L1GS_213113_19890201
LT04_L1GS_015112_19900124	LT04_L1GS_213114_19890201
LT04_L1GS_213115_19890116	LT04_L1GS_125109_19891226
LT04_L1GS_213116_19890201	LT04_L1GS_221109_19900127
LT04_L1GS_213117_19890321	LT04_L1GS_219112_19891212
LT04_L1GS_215115_19890130	LT04_L1GS_215112_19881229
LT04_L1GS_215116_19890130	LT04_L1GS_215111_19881229
LT05_L1GS_169118_19860301	LT04_L1GS_221111_19891124
LT05_L1GS_169119_19860301	LT04_L1GS_221110_19900127
LT05_L1GS_169120_19860213	LT04_L1GS_217111_19890128
LT05_L1GS_169121_19860213	LT04_L1GS_219110_19891126
LT05_L1GS_180117_19860226	LT04_L1GS_219111_19891126
LT05_L1GS_180118_19860226	LT04_L1GS_218110_19890220
LT05_L1GS_180119_19860226	LT05_L1GS_219109_19910124
LT05_L1GS_183119_19860215	LT04_L1GS_223111_19891224
LT05_L1GS_183120_19860215	LT04_L1GS_004111_19891226
LT05_L1GS_183121_19860215	LT04_L1GS_226112_19880210
LT05_L1GS_199116_19860215	LT04_L1GS_229112_19890201
LT05_L1GS_199117_19860215	LT05_L1GS_232111_19910220
LT05_L1GS_199118_19860215	LT04_L1GS_001111_19891221
LT05_L1GS_202115_19860220	LT04_L1GS_221112_19890124
LT05_L1GS_202116_19860220	LT04_L1GS_221113_19890124
LT05_L1GS_204116_19860306	LT04_L1GS_223112_19891224
LT05_L1GS_204117_19860306	LT04_L1GS_229111_19890201
LT05_L1GS_204118_19860306	LT04_L1GS_229112_19890217
LT04_L1GS_187117_19890227	LT05_L1GS_232112_19910220
LT04_L1GS_204114_19891219	LT04_L1GS_233123_19891128
LT04_L1GS_190120_19890131	LT04_L1GS_021119_19891115
LT04_L1GS_190119_19890131	LT04_L1GS_007118_19881212
LT04_L1GS_185117_19890301	LT04_L1GS_233122_19891128
LT04_L1GS_128108_19891129	LT04_L1GS_030115_19900218
LT04_L1GS_128109_19891129	LT05_L1GS_016119_19870115
LT04_L1GS_128110_19891129	LT04_L1GS_014117_19900218
LT04_L1GS_128111_19891129	LT05_L1GS_025117_19870114
LT04_L1GS_128112_19891129	LT04_L1GS_021118_19900203
LT04_L1GS_116107_19890314	LT04_L1GS_025117_19891229
LT04_L1GS_118107_19890312	LT04_L1GS_019118_19890117
LT04_L1GS_120106_19900124	LT04_L1GS_014118_19900218
LT04_L1GS_120107_19900124	LT04_L1GS_007119_19881212

LT04_L1GS_122107_19891205	LT04_L1GS_024114_19881219
LT04_L1GS_122108_19891205	LT04_L1GS_024115_19881219
LT04_L1GS_124107_19900120	LT04_L1GS_024116_19890309
LT04_L1GS_124108_19900120	LT04_L1GS_025119_19891229
LT04_L1GS_124109_19900120	LT04_L1GS_025118_19891229
LT04_L1GS_120108_19900124	LT04_L1GS_030114_19900218
LT04_L1GS_125110_19891108	LT04_L1GS_030117_19900202
LT04_L1GS_125111_19891108	LT04_L1GS_035116_19900205
LT04_L1GS_125112_19900212	LT04_L1GS_035117_19900205
LT04_L1GS_125113_19900212	LT04_L1GS_030116_19900202
LT04_L1GS_128113_19891231	
LT04_L1GS_129110_19890309	
LT04_L1GS_131109_19891118	